31 Mar 2023

# Investigation of Corrosion Mechanism of Ribbed Mild Steel Bars Coated with Magnesium Potassium Phosphate Cement Paste

Fan Zhang

John J. Myers
*Missouri University of Science and Technology*, jmyers@mst.edu

Wenyu Liao

Cun Hui

*et. al. For a complete list of authors, see https://scholarsmine.mst.edu/civarc_enveng_facwork/2384*



## Recommended Citation

F. Zhang et al., "Investigation of Corrosion Mechanism of Ribbed Mild Steel Bars Coated with Magnesium Potassium Phosphate Cement Paste," *Construction and Building Materials*, vol. 371, article no. 130639, Elsevier, Mar 2023.
The definitive version is available at https://doi.org/10.1016/j.conbuildmat.2023.130639

Construction and Building Materials 371 (2023) 130639

Contents lists available at ScienceDirect

Construction and Building Materials

journal homepage: www.elsevier.com/locate/conbuildmat

# Investigation of corrosion mechanism of ribbed mild steel bars coated with magnesium potassium phosphate cement paste

Fan Zhang [a], John J. Myers [a,*], Wenyu Liao [a], Cun Hui [b], Hongyan Ma [a]

[a] Department of Civil, Architectural, and Environmental Engineering, Missouri University of Science and Technology, Rolla, MO 65401, USA
[b] School of Architecture and Civil Engineering, Zhongyuan University of Technology, Zhengzhou, Henan 450007, China

ARTICLE INFO

*Keywords:*
Magnesium potassium phosphate cement
Ribbed steel bars
Coating
Anti-corrosion
Double protection system

ABSTRACT

This study investigated the anti-corrosion performance of magnesium potassium phosphate cement (MKPC) paste applied to the surface of ribbed mild steel bars – which was exposed to simulated accelerated corrosive environment. Four electrochemical approaches were used including open-circuit potential (OCP), electrochemical impedance spectroscope (EIS), polarization resistance (PR) and potentiodynamic polarization (PDP) over a period of 5376 h (224 days). Moreover, visual inspection, optical microscope, and scanning electron microscopy (SEM) with energy dispersive spectroscopy (EDS) were used to assess the extent of corrosion on the samples. To understand the mechanism of corrosion protection of the coating system, X-ray photoelectron spectroscopy (XPS) was employed to characterize the chemical groups on the surface of mild steel, and the chemical changes in the coating layer were characterized using thermogravimetric/differential thermal analysis (TG/DTA) and X-ray diffraction (XRD). The MKPC paste coated bars were compared with not only uncoated bars, but also bars coated with ordinary Portland cement (OPC) that is known to passivate steel due to its high alkalinity. Results indicated that MKPC paste coating layer could effectively protect the ribbed mild steel bars, and its protectiveness significantly surpassed that of OPC. Both the de-passivation effects of chloride ions and carbonation of the OPC resulted in relatively severe corrosion of the OPC coated bars during the long exposure duration; while the anti-corrosion merit of the MKPC paste coating layer could be attribute to a double-protection system– the dense microstructure of MKPC and the formation of an iron (III) phosphate passivation layer between the substrate steel and the MKPC paste coating layer.

## 1. Introduction

Corrosion of steel poses the largest threat and deterioration problem to mild steel reinforcement in concrete structures all over the world. Apart from common corrosion issues due to general exposure to oxygen and moisture, the corrosion of steel reinforcement in concrete can be accelerated by two major factors, i.e., the ingress of chloride ions, and carbonation of the concrete [1]. In the United States alone, the total direct cost of corrosion is estimated at $276 billion per year, which is 3.1 % of the gross domestic product (GDP) [2]. With the continued construction of reinforced concrete (RC) structures, this number will grow larger. Considering the difficulties and costs of corrosion repairs, preventing corrosion and/or delaying the corrosion rate from the onset are a much more desirable option for RC structures. According to the famous de Sitter's law of Fives [3], $1 extra investment in steel protection is equivalent to roughly $5, $25, and $125 repairs in the initiation, propagation, and advanced propagation stages of steel corrosion. Therefore, a more robust investment to prevent or delay corrosion is well worth the initial investment.

Currently, the most efficient and common method to protect mild steel bars in an external corrosive environment is by building a chemical or physical barrier between the steel and environment. Improving the anti-corrosion performance of reinforcement in concrete can be achieved by modifying the ordinary Portland cement's cementitious protective cover (i.e., using a specific type cement, adding a superplasticizer or other admixtures [4,5] and changing the water-cement ratio, or by using the cathodic method to protect the bars (i.e., hot-dip galvanized coating [6] and magnesium alloy anode [7]) or by providing a special coating over bars before casting fresh concrete, such as fusion bonded epoxy and enamel coating [8]. In addition, another mechanism is to form a passive film on the steel surfaces to prevent the corrosion process. One of the most common is the passive film formed

* Corresponding author at: 325 Butler-Carlton Hall, 1401 N Pine St, Rolla, MO 65409, USA.
*E-mail address:* jmyers@mst.edu (J.J. Myers).

https://doi.org/10.1016/j.conbuildmat.2023.130639
Received 14 September 2022; Received in revised form 4 January 2023; Accepted 3 February 2023
Available online 24 February 2023

due to high alkalinity from the ordinary Portland cement system [9].

However, current methods of preventing corrosion have different limitations or flaws. Incomplete coating over the entire surface of the bars will lead to small pits by human error, which affects the long-term performance of corrosion resistance [10–12]. Meanwhile, with the presence of penetration ions, the under film corrosion will lead to a weak bond between the substrate steel and coating layer [13]. Moreover, the process of applying a hot-dip galvanized coating is impossible to apply manually. The coating must be applied in an industrial environment and if damaged the coating cannot be repaired, only the whole element must be reapplied. Furthermore, when the pH value of pore solution of ordinary Portland cement's cementitious materials reaches a level up to 13.2, zinc dissolves accompanied by the release of hydrogen gas [14]. With the accumulation of this gas, the bond performance between the steel bar and protective cover become weaker [14,15].

Magnesium potassium phosphate cement (MKPC) is made of dead-burned magnesium oxide (MgO), the calcination temperature is 1000–1500 ℃ (1832 to 2732 °F), and potassium dihydrogen phosphate, $KH_2PO_4$ (KDP) through an acid-based chemical reaction [16]. Compared to traditional concrete, MKPC possess many beneficial characteristics, such as high early-strength, favorable bond strength to old concrete and steel, and a low permeability with good durability characteristics [17–19]. Therefore, magnesium potassium phosphate cement holds great promise as a fast repair material for reinforcement concrete structures due to its fast-setting nature and good steel corrosion inhibition capacity [20]. The principal chemical reaction of MKPC may be described as follows (1) [21]:

$$MgO + KH_2PO_4 + 5H_2O \rightarrow MgKPO_4 \bullet 6H_2O \quad (1)$$

In recent years, during the investigation of corrosion resistance mechanisms of magnesium phosphate cement (MPC) based materials, it demonstrated a good anti-corrosion performance and was thought to develop a passive layer to protect bars [22]. Furthermore, similar studies were investigated by other researchers. Jun et al. reported that MPC coating can significantly improve the erosion resistance of the concrete to sulfate [23]. Wang et al. demonstrated that the anti-corrosion ability was improved by adding silica fume to the MKPC coating constituents [24]. Meanwhile, the wollastonite modified MPC showed lower compressive strength loss when the samples exposed to NaCl freeze–thaw cycles and dry-wet cycles in NaCl solution [25]. The MPC coating also can serve as a good physical barrier against water invasion and reducing the ions transfer due to its low permeability and good durability properties. Meanwhile, the favorable bond strength of MPC is a key factor in practice to protect the bars without peeling. Therefore, the magnesium phosphate cement paste could be a good anti-corrosion coating by producing a chemical barrier on the steel surface and providing a physical barrier to stop the ingress of moisture, oxygen and other corrosive ions. In order to investigate the anti-corrosion performance of MKPC for ribbed bars, this research explored the magnesium potassium phosphate cement paste coating system, its corresponding anti-corrosion mechanism and its formation process.

In this research, a systematic study was carried out to investigate magnesium potassium phosphate cement coating's anti-corrosion mechanism, the characterization of the magnesium potassium phosphate coating layer and the new chemical products formed between magnesium potassium phosphate coating layer and substrate mild steel. Results from electrochemical testing were used to investigate the changing trend of impedance as well as the electrochemical characterization of corrosion rate of bars coated with different coatings. Then, the macro and micro morphology, composition and microstructure of coating layer surface layer was investigated and discussed through visual inspecting, optical microscope and scanning electron microscopy (SEM) with energy dispersive spectroscopy (EDS). Finally, the chemical group at the surface of substrate steel was characterized by XPS. The formation process of the protective passive layer was proposed by charactering and analyzing the chemical composition of the magnesium potassium phosphate cement paste coating layer by XRD and TG/DTA. By analyzing all data obtained from each experiment, its anti-corrosion performance was analyzed and discussed in this research study.

## 2. Experiment details

### 2.1. Materials

A dead burned magnesia (DBM) and a chemical reagent of 99 % purity potassium dihydrogen phosphate ($KH_2PO_4$, KDP) were supplied by Martin Marietta Magnesia Special Ties, LLC from Manistee MI, United States and ICL Specialty Fertilizers-Americas from Summerville SC, United States, respectively. The Type I Portland cement (PC) supplied by the LafargeHolcim ltd building materials company was used to produce specimens coated with ordinary Portland cement paste as one comparison group. This group was compared with the specimens coated in magnesium potassium phosphate cement paste. The chemical composition, which was tested using an X-ray fluorescence spectrometer (Oxford X-supreme 8000), for all oven-dried materials used in this study are shown in Tables 1–3. The measurement time lasted 200 s at the 40.00 mm (1.57 in.) aluminum cups. The #4 ribbed mild steel rebar with a diameter of 12.70 mm (0.50 in.) was used in order to investigate properties of steel corrosion resistance under the protection of OPC and MKPC coating in a full-size, real-world bar application.

### 2.2. Preparation of coatings and specimens

#### 2.2.1. Preparation of coating group and 3.5 wt% NaCl corrosion solution

In this research, three testing sample conditions were investigated: Group I (UN) is the bare mild steel bar without any surface treatment. The samples of Group II (OPC) were coated with ordinary Portland cement paste. Group III (MKPC) is mild steel bar coated with magnesium potassium phosphate cement paste. The MgO to KDP (M/P) mole ratios and water to binder (w/b) ratios of the MKPC paste using in the research are 6 and 0.18, respectively, and the retarder was not used in this research. Since the compressive strength of MKPC paste was about 27.58 MPa (4000 psi) at the seven days testing age, the same compressive strength for OPC paste was needed, thus, the 0.38 w/b ratio for OPC paste was used in this research.

The 3.5 wt% NaCl corrosion solution was made by mixing purified sodium chloride with deionized water, so it means that the chloride concentration is about 0.6 mol/L. After magnetic stirring in an indoor environment [temperature is 20 ± 2 ℃ (64 to 72 °F) and air humidity is 55 ± 10 %], all samples were immersed into this solution. Before the electrochemical test, conductivity and temperature of the 3.5 wt% NaCl corrosion solution were determined by a Hanna Instruments HI5522 Meter. These two values stabilize at 55.0 ± 5 mS/cm and 20 ± 2 ℃ (64 to 72 °F), respectively. During the entire EC test period, the conductivity and temperature of the corrosion solution was measured in the same way, the values kept stable, and no changes occurred. Furthermore, during the EC test, the pH value of corrosion solution also was monitored.

#### 2.2.2. Electrochemical specimens

The two ends of an 89 mm (3.5 in.) #4 ribbed mild steel bar were encased in two PVC tubes containing marine epoxy resin. Each of PVC tubes was 31.8 mm (1.25 in.) and the actual coating layer length of sample steel bar was 50.8 mm (2 in.) in the middle portion. Therefore, the testing surface area was approximately 20.26 $cm^2$ (3.14 $in^2$). A copper wire was electrically connected at one end of the mild steel bar. The specimen diagram is shown in Fig. 1.

All the mild steel bars used to make specimens were cut from same rebar and the surface of these bars were treated by using sandpaper, and polishing sequentially from 240, 600 and 1200 grit. Even though the surface were polished, minor oxidation may have occurrence prior to the application of coating paste over the substrate steel bars. Three groups of

**Table 1**
Chemical composition of the dead-burned magnesia (Weight %).

| MgO | $SiO_2$ | CaO | $Al_2O_3$ | $Na_2O$ | $Fe_2O_3$ | $SO_3$ | $P_2O_5$ | other |
|---|---|---|---|---|---|---|---|---|
| 91.897 | 4.704 | 1.157 | 1.073 | 0.652 | 0.233 | 0.131 | 0.107 | 0.046 |

**Table 2**
Chemical composition of the potassium dihydrogen phosphate (Weight %).

| $P_2O_5$ | $K_2O$ | $SiO_2$ | $Na_2O$ | $Al_2O_3$ | $SO_3$ | CaO | other |
|---|---|---|---|---|---|---|---|
| 53.607 | 41.979 | 2.514 | 0.840 | 0.625 | 0.209 | 0.170 | 0.056 |

three specimens were used as follows:

a. The mild steel bar specimens are uncoated. They were cleaned with pure-100 isopropyl alcohol solution in an ultrasonic cleaner for 2 min, then dried under a vacuum drying oven. This kind of specimens is denoted as UN.
b. The OPC paste was coated on the mild steel bar specimens using a brush and with a curing time of 7 days at the indoor environment [temperature is 20 ± 2 ℃ (64 to 72 °F) and air humidity is 55 ± 10 %]. The thickness of the OPC coating layer is 0.7 ± 0.1 mm (0.028 ± 0.0039 in.). The changes values of coating layer shown in the Fig. 2. This kind of specimens is denoted as OPC.
c. The magnesium potassium phosphate cement paste was coated on the mild steel bar by using a brush and had a curing time of 7 days at the same indoor environment as the OPC specimens. The thickness of the magnesium potassium phosphate cement paste coating layer is 0.5 ± 0.1 mm (0.020 ± 0.0039 in.). The changes values of coating layer shown in Fig. 2. The thickness of its coating layer is thinner than the thickness of the OPC coating due to different viscosity and flowability. This kind of specimens is denoted as MKPC.

*2.2.3. The preparation of morphology and microstructure of the samples*

After the 5376 h (224 days) EC test, the OPC and MKPC coating part from each specimen were immersed in pure-100 isopropyl alcohol solution for 3 and 1 days, respectively, to stop hydration. Then, the OPC samples were vacuum dried at 60 ℃ (140 °F) for 24 h, and MKPC samples were vacuum dried at 30℃ (86°F) for 24 h. Some of them were ground to pass through a 75 μm (0.00295 in.) sieve for the TG/DTA and XRD test, and the remaining small pieces were retained for the optical microscope test. For visual inspection, TG/DTA and XRD tests, a total of four samples were conducted for each test. One part is 7 days curing time sample before the EC test for OPC and MKPC, and another is sample after the 5376 h (224 days) EC test for OPC and MKPC. However, in order to inspect the inner and outer surface of samples after the 5376 h EC (224 days) test, besides the coating layer from samples before the EC test, the outer coating portion in contact with the corrosion solution and inner coating portion that was in direct contact with the substrate steel bar was separately observed using an optical microscope. In addition, only the seven days curing time MKPC sample underwent the SEM test because the sample after the EC test did not meet the SEM test requirement. This sample was cut from the same mild steel rebar coated with magnesium potassium phosphate cement paste and sealed into white resin. Then, it was ground sequentially from 6 μm ($23.622e^{-5}$ in.) size, 3 μm ($11.811e^{-5}$ in.) size, 1 μm ($3.937e^{-5}$ in.) size 0.5 μm ($1.969e^{-5}$ in.) size to 0.25 μm ($0.984e^{-5}$ in.) size diamond polishing compound, cleaned with pure-100 isopropyl alcohol solution in an ultrasonic cleaner for 20 s, and dried with an air heater in the interval between replacing diamond polishing compounds. The specimens for the XPS test were conducted over the mild steel surface peeling the MKPC coating part before and after the 5376 h (224 days) EC test, and they were cleaned with pure-100 isopropyl alcohol solution. Then, dried at 30 ℃ (86 °F) in an electric vacuum drying oven for 24 h.

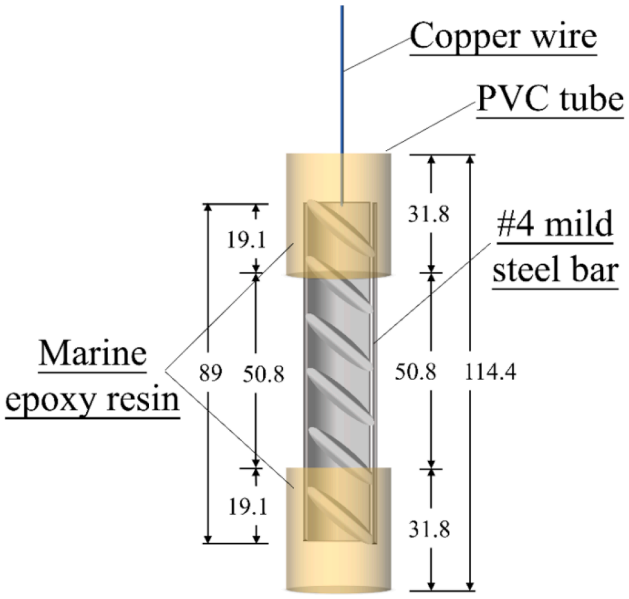


**Fig. 1.** Geometry of rebar samples (unit: mm).

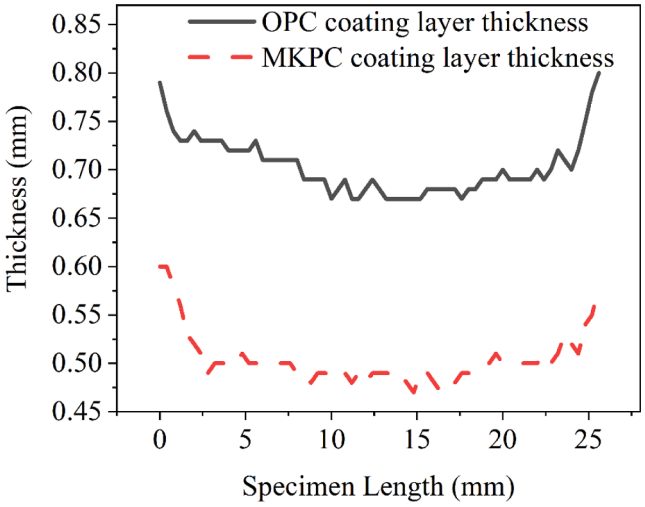


**Fig. 2.** Coating layer thickness.

**Table 3**
Chemical composition of the Type I cement (Weight %).

| CaO | $SiO_2$ | $Al_2O_3$ | $Fe_2O_3$ | $SO_3$ | MgO | $K_2O$ | $TiO_2$ | other |
|---|---|---|---|---|---|---|---|---|
| 67.878 | 19.354 | 4.045 | 3.449 | 2.344 | 1.812 | 0.652 | 0.194 | 0.272 |

### 2.3. Test method

#### 2.3.1. Electrochemical (EC) test

The electrochemical measurements and data were performed and collected by using a typical three-electrode setup named Gamry Interface 1000-potentiostat. A 25.4 × 25.4 × 0.254 mm (1 × 1 × 0.01 in.) platinum sheet, a saturated calomel electrode (SCE) and the prepared specimens as shown in Fig. 1 were used as counter electrode (CE), reference electrode (RE) and working electrode (WE), respectively. The EC test setup is shown in Fig. 3.

All electrochemical data collected and presented in this paper refer to SCE. All data were collected for increasing immersion times at 5 h, 168 h (7 days), and measuring data every 168 h (7 days) to 1344 h (56 days), then, collecting data every 672 h (28 days) to 5376 h (224 days). All prepared working electrode specimens were immersed in 3.5 wt% salt solution consisting of distilled water and purified sodium chloride. During the entire test process, the following tests were conducted. The open-circuit potential (OCP) test started after the samples were immersed into 3.5 wt% NaCl corrosion solution for 5 h. OCP were first recorded for a period of 3600 s. The remaining test lasted until reaching to 5 mV/hour, as the immersion time increased, the OCP's value tended to be stable and had no significant change. The electrochemical impedance spectroscopy (EIS) [30] was tested with an applied sinusoidal potential wave of 10 mV amplitude and frequency ranging from 100 kHz to 0.01 Hz at a sampling of 6 data cycles/decade after the OCP test. After the EIS, the polarization resistance (PR) test starts. It was carried out from −15 mV to 15 mV at a scan rate of 0.166 mV/s. Representing the slope of the polarization curves, the $R_p$ can be calculated by following equation (2):

$$R_p = \Delta V/\Delta i \tag{2}$$

where ΔV and Δi represent the voltage and current increments, respectively [31]. In order to minimize the error of EIS results influenced by the Potentiodynamic Polarization (PDP) test, the same mixture ratio sample at same corrosion situation were tested with the PDP method [32] from $E_{ocp}$-300 mV to $E_{ocp}$ + 1200 mV with a scanning rate of 5 mV/s at 5 h, 1344 h (56 days) and 5376 h (224 days). The EC-lab software was used to fit the electrical equivalent circuit (EEC) model into the collected EIS data from the Gamry electrochemical workstation.

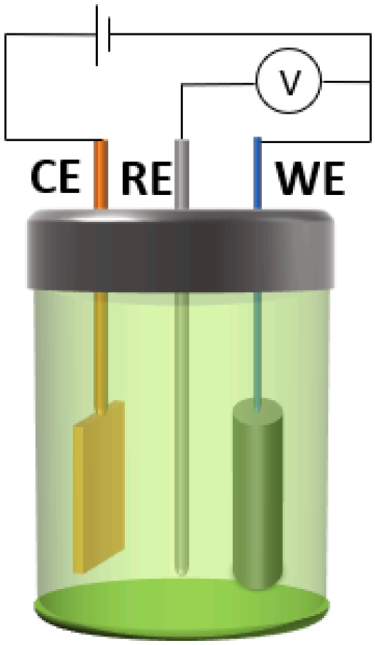


**Fig. 3.** Three-electrode setup.

#### 2.3.2. Corrosion morphology

The prepared specimens were from the coating portion of OPC and MKPC specimens before and after the 32 weeks EC test, which were then examined by Hirox RH-2000 3D digital microscope with enlargement of 100 and 1500 times. The parts of samples included the seven days curing paste before EC test, and the inner and outer of coating part after the 5376 h (224 days) EC test.

#### 2.3.3. Scanning electron microscopy (SEM)

The prepared specimen underwent the SEM test using a Helios Nanolab 600 coupled to an energy dispersive X-ray spectroscopy (EDS), which was used to analyze the distribution of chemical elements of the cross section of specimens from the inner substrate mild steel part to outside coating part. It was imaged with 15 kV accelerating voltage and 0.34nA current with enlargement of 1500 times.

#### 2.3.4. X-ray photoelectron spectroscopy (XPS) test

The surfaces of substrate steel of MKPC specimens underwent the XPS test to analyze the chemical group formed due to the reaction between MKPC paste and mild steel rebar. X-ray photoelectron spectroscopy were recorded using a Thermoscientific Nexus system. The radiation source was monochromatic Al Kα radiation (hv = 1486.6 eV), and takeoff angle was 0°. The high-resolution spectra of C 1 s, O 1 s, Fe 2p and P 2p were measured and the survey scans was in the range of 0 ~ 1100 eV (binding energy). The calibration value C 1 s peak (284.6 eV) was applied on the binding energies of the measured XPS spectra.

#### 2.3.5. Thermogravimetry/Differential thermal analysis (TG/DTA) test

The TG/DTA test was conducted on the prepared treated powder by using a TA instruments SDT Q600 under nitrogen atmosphere with flowing rate of 40 ml/s. These powders were heated from room temperature to 30 ℃ (86 °F), and keep it for 5 mins, then heated to 980 ℃ (1796 °F) for OPC specimens and 850 ℃ (1562 °F) for MKPC specimens at a heating rate of 10 ℃/min in an aluminum crucible.

#### 2.3.6. X-ray diffraction (XRD) test

To analyze the chemical composition of cementitious coating, X-ray diffraction (XRD) data of prepared specimens were collected by a Panalytical X'pert Pro MPD diffractometer, using CuKα radiation (λ = 1.54 Å). The patterns were examined at indoor environment with 2θ ranging from 5° to 90° for 15 mins. The phase compositions were identified with the assistance of X'pert high score Plus software.

## 3. Results and discussion

### 3.1. Open-circuit potential (OCP)

The first 3600 s' evolution in open-circuit potential of three specimens after they have been immersed into 3.5 wt% NaCl corrosion solution for 5 h are presented in Fig. 4.

Compared with the OPC and MKPC, the variation in open-circuit potential's value of UN significantly decreased, especially for UN#1 in the first 2000 s, the value decreases from −0.55 to −0.6 V/SCE, UN#2 and UN#3 slightly decreased. This is attributed to the rapid growth and enlargement of active corrosion sites on the surface of bare mild steel bar's surface [33]. The OCP's value of all three UN specimens tend towards −0.61 V/SCE and stability within the 3600 s. For the OPC's and MKPC's value, the corrosion system was probably stable at the first five hours. Since the variation of open-circuit potential's value of OPC and MKPC change very little after being immersed them into corrosion solution for five hours plus one more hour for testing. Compared to the UN samples, the coating part played a role in stabilizing the value due to limiting the charge transfer to some degree.

In addition, at the end of tests after 3600 s of immersion, the average open-circuit potential's value kept stable at around −0.567 V/SCE for the OPC coating and −0.83 V/SCE for the MKPC coating. This is because

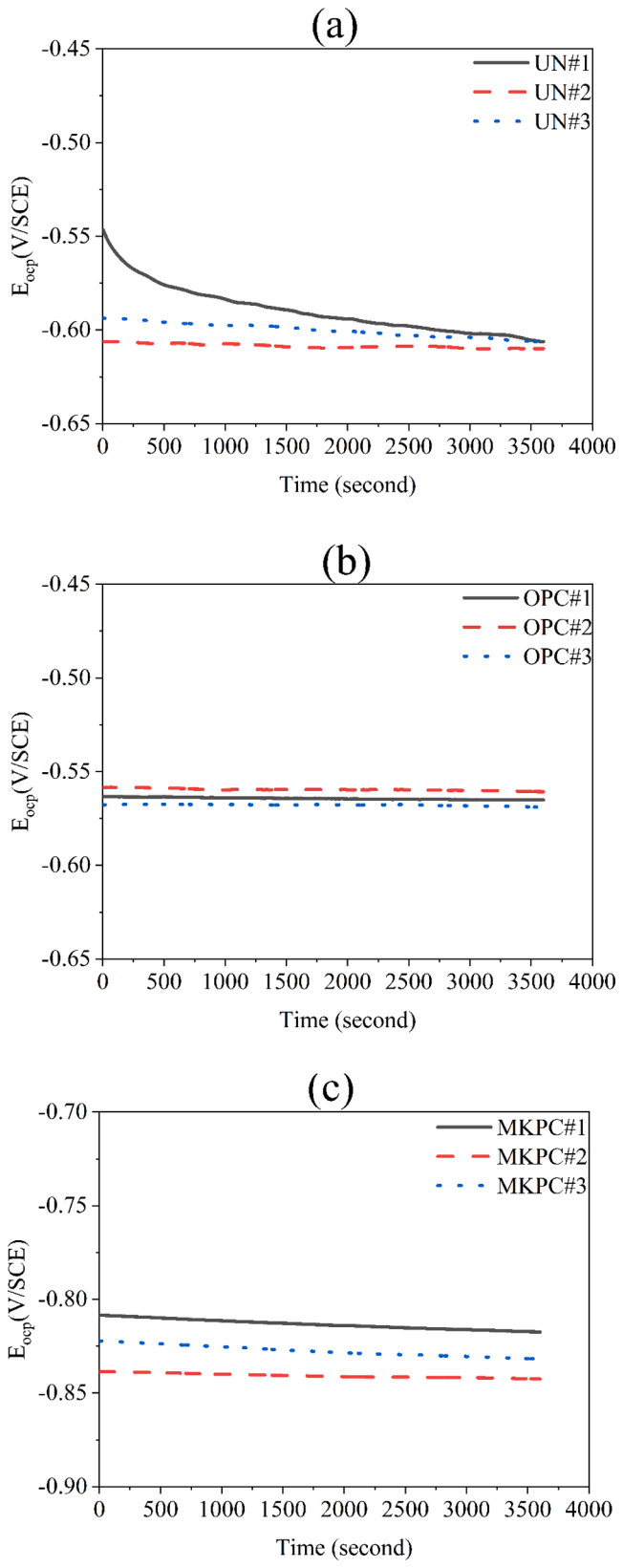


**Fig. 4.** Open-circuit potential evolution over time for (a) uncoated, (b) OPC coated and (c) MKPC coated.

the corrosion activation systems of the specimens and the corrosion solution trend to sable. According to the ASTM C876[34], if potentials over an area are more negative than −0.2735 V/SCE (-0.35 V/CSE), there is a greater than 90 % probability that reinforcing steel corrosion is occurring in that are at the time of measurement. According to test results, all recorded open-circuit potential's values are more negative than −0.2735 V/SCE after being immersed into corrosion solution for 6 h. This is because the OPC samples, like all other cementitious materials, are not the perfect insulator and contain a pathway for the holidays through the coating area, which lead to charged ion transported and exchanged through these holidays. When the steel was exposed to the corrosion solution containing the chloride ion at this severe corrosive testing environment, the corrosion immediately started [35]. Meanwhile, the 7 days curing time for OPC coating samples also probably influence the open-circuit potential's value. However, even though the open-circuit potential's values of MKPC sample were also lower than the threshold of −0.2735 V/SCE and the open-circuit potential's values of UN and OPC, the steel corrosion degree is far slighter than other two according to corrosion morphology after EC test. This is probably due to the reaction between the iron and phosphate radical rather than the ordinary steel corrosion reaction [36], which is not the same as the corrosion process. Meanwhile, the MKPC-based cementitious materials also contain holidays. These holidays may be also a weak, which lead to corrosion occurring. Therefore, all these values are lower than the threshold of −0.2735 V/SCE.

In addition, the collected data from the specimens in same group of long-term corrosion of open-circuit potential value in same situation were recorded and exhibited similar trend, and only the representative results of each group have been presented in this paper. Fig. 5 shows the open-circuit potential evolution of the three groups from 5 to 5376 h (224 days) in every 168 h (7 days) for the first 1344 h (56 days), then, in every 672 h (28 days) until the end of test at 5376 h (224 days).

For UN specimens, the open-circuit potential value reduced from around −0.61 V/SCE at 5 h to around −0.73 V/SCE at 1008 h (42 days) and almost kept stable until to the test end. For the OPC and MKPC's open-circuit potential value, they tend towards stability after 1008 h. At the time of 5376 h (224 days), the OPC's value is similar to the bare bar's value. This is because the steel bar has already corroded leading to peeling compromising the coating layer. Thus, some surface of substrate steel of OPC samples was directly exposed to the corrosion solution like the UN samples. Furthermore, during the first 1008 h, the open-circuit potential value changed a lot for OPC samples, this is due to the chloride iron that was passed through the thin coating part and involved in corrosion processes [37]. After that period, the values stabilized, and the open-circuit potential reached an equilibrium state. Even though the

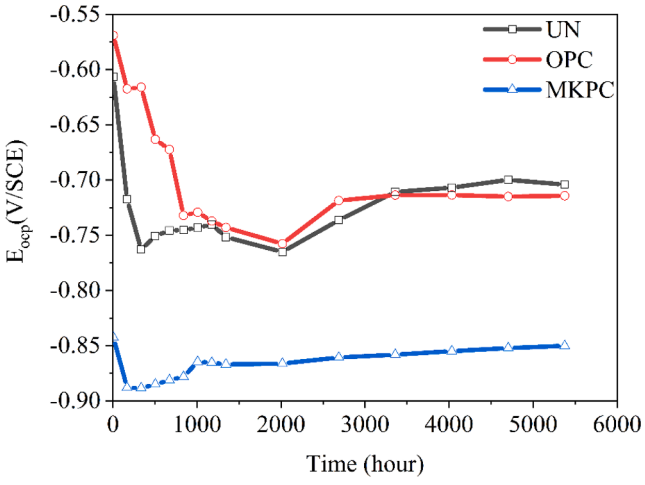


**Fig. 5.** Open-circuit potential evolution over time for uncoated, OPC coated and MKPC coated.

open-circuit potential's value of MKPC is the lowest of these three samples, its value is the most stable, which means the chemical reactions occurred on the bars surface of MKPC samples from first test to the end of test was not significantly affected by the corrosion solution. This also illustrated that the MKPC samples show a better anti-corrosion performance than OPC samples.

### 3.2. Electrochemical impedance spectroscopy (EIS)

Since the specimens of each group exhibited similar results, Fig. 6 shows the one representative impedance diagrams in three groups in the format of Bode and Nyquist plots. These points in the figure represent tested data from the electrochemical workstation and the solid line connecting all points represents the fitting results using an equivalent electrical circuit (EEC) model as shown in Fig. 7. Meanwhile, in order to better illustrate the connection between the EEC models with Nyquist

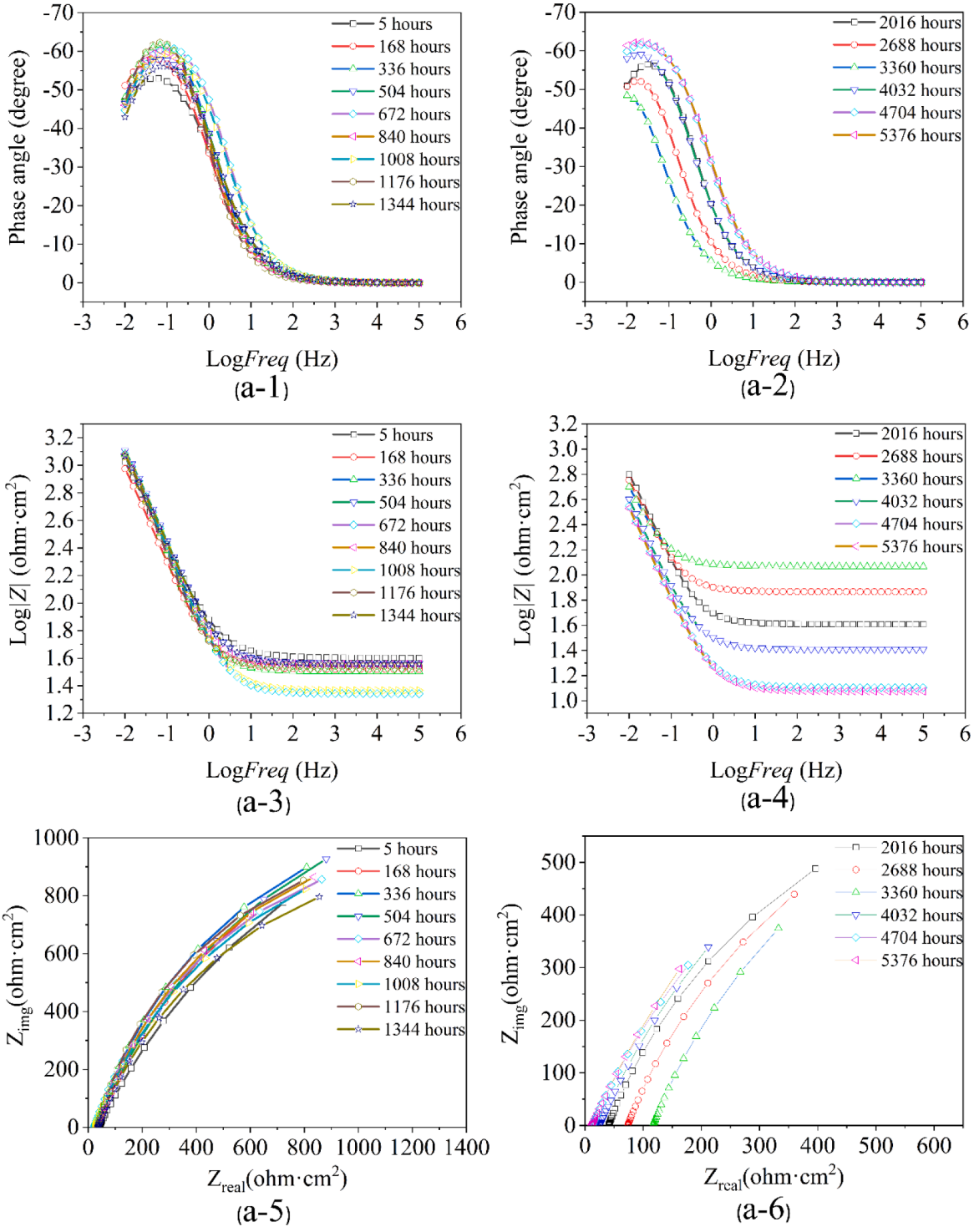


**Fig. 6.** EIS diagrams (number 1, 2, 3 and 4: Bode plots; number 5 and 6: Nyquist plots) for: (a) uncoated, (b) ordinary Portland cement coating and (c) magnesium potassium phosphate coating.

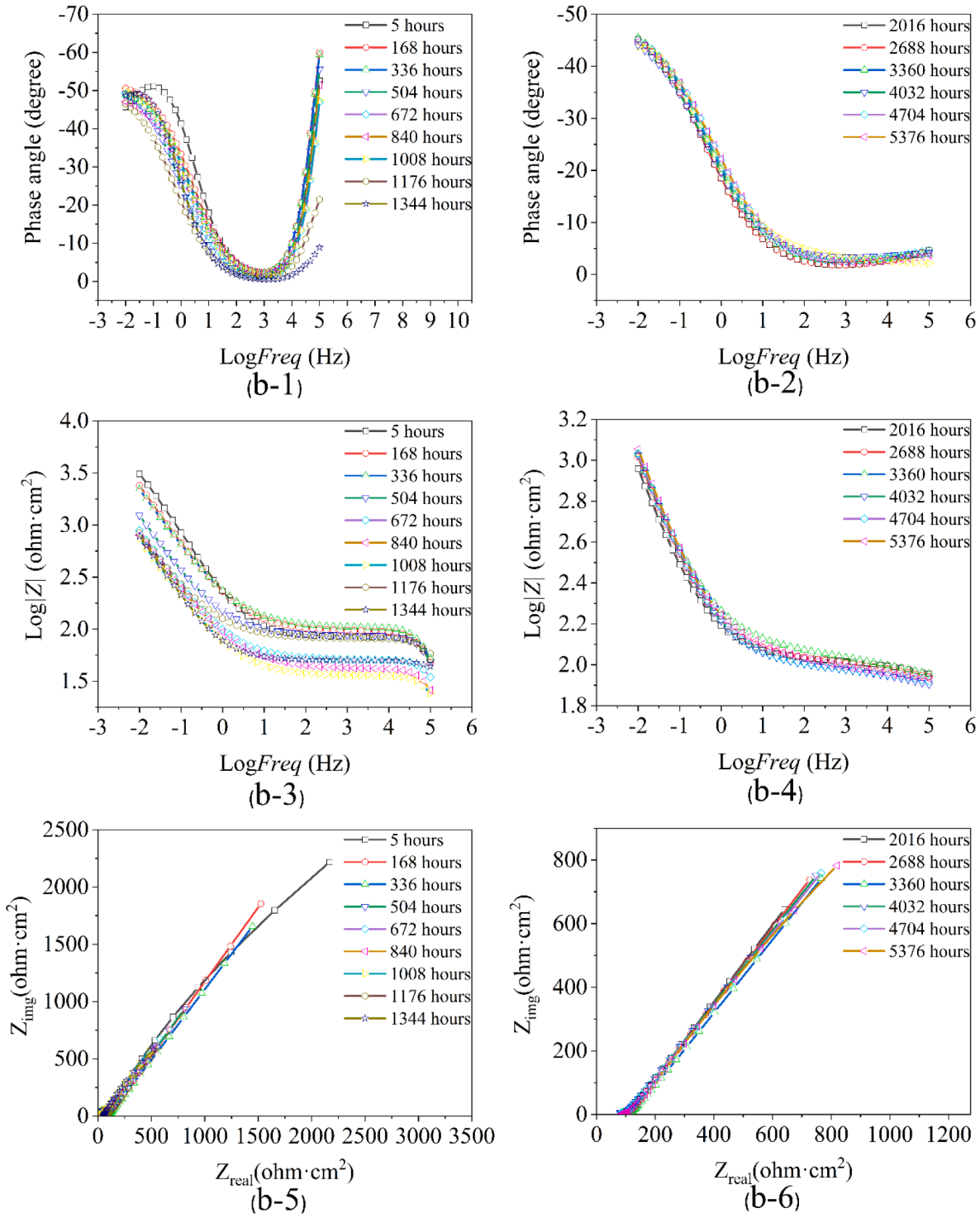


**Fig. 6.** (*continued*).

plot, the Nyquist data at 5 h and related EEC-III-a model will be used as an example as shown in Fig. 8. The frequency, constant phase element and corresponding Nyquist plots are shown. More detailed information is presented in the following part.

The first two Bode plots of Fig. 6(a-1) to (a-4) only present one time constant which is caused by the double layer capacitor effect and surface polarization effects [38]. This is typical uncoating corrosion steel specimens and these corrosion conditions and their corresponding model have already been well studied [39–41]. The interface between the corrosion solution and the substrate steel represents one double layer capacitance and charger transfer resistance. Meanwhile, the Fig. 6(a-3) and (a-4) of bode plots in show that the impedance at low frequency decreases with the increased immersed time due to the corrosion degree increase. For Nyquist plots, $Z_{real}$ is the resistance consisted by electrolyte resistance and corrosion resistance and $Z_{img}$ relates to the capacitive due to the double layer capacitance effects [42]. Fig. 6(a-5) and (a-6) are Nyquist plots, which are consistent with the bode plots, whether the trend of the impedance with the time elapsed or characteristic of one-time constant shown in these figures. Based on the analysis and observation, the initial fitting model should be the EEC-I-a. With the corrosion

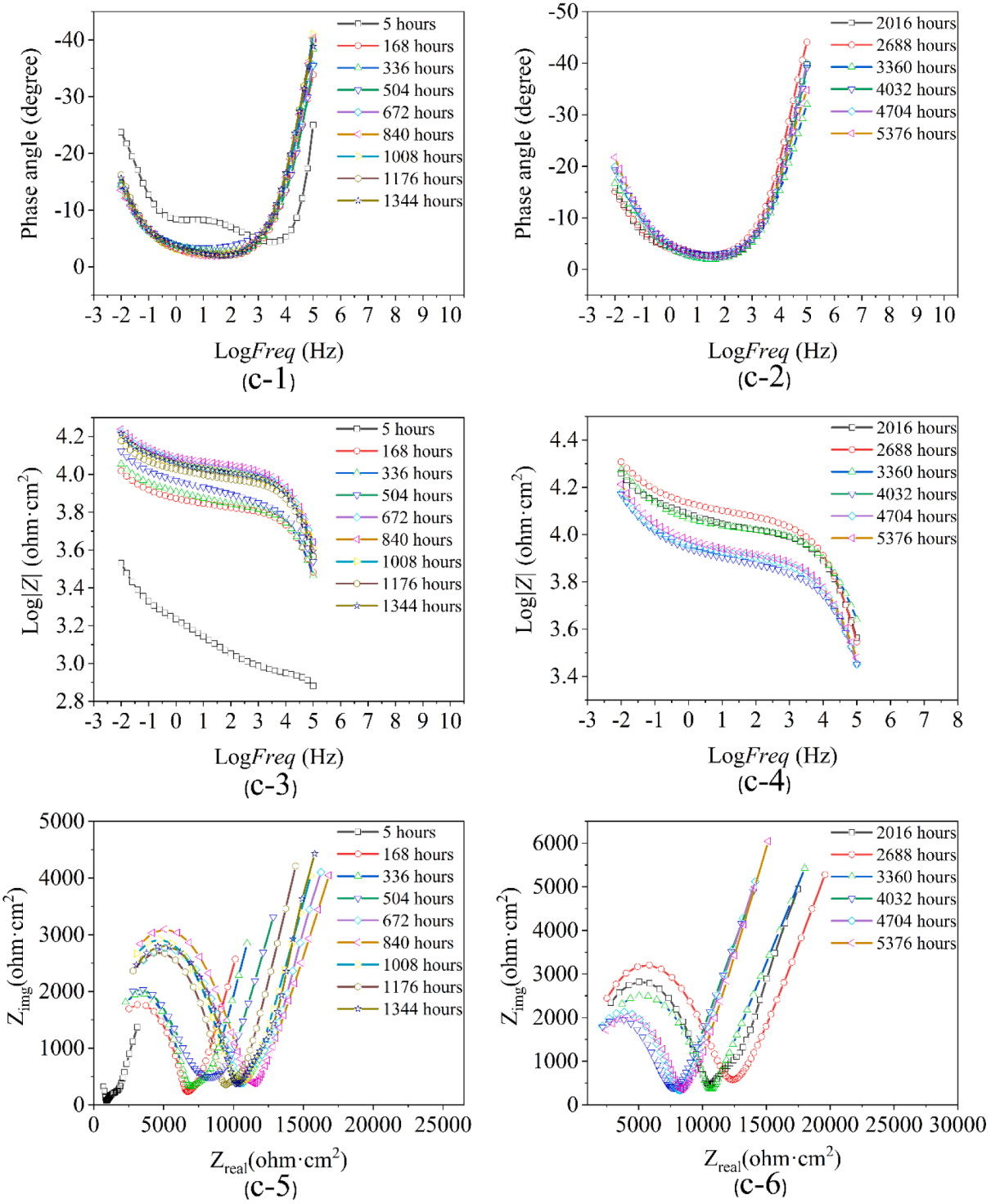


**Fig. 6.** (*continued*).

occurring, the uncoated corrosion steel specimens can be simulated to the Fig. 7 EEC-I-b model. As this sample is without coating, the diffusion control appears at the low frequency area after the first measured data, a result of the formation and accumulation of the corrosion products on the surface of substrate steel. Thus, the Warburg diffusion impedance *W* was used in EEC-I-b models, same as EEC-II-b and III-b model. In EEC-I model, the $R_s$ corresponds to the solution resistance, $CPE_{dl}$ represents double layer capacitance, and $R_{ct}$ is the charge transfer resistance. The formation of the double layer capacitance, which is not a perfect capacitor, is due to irregularities in the exposed steel surface, such as rough surface, non-uniform distribution of corrosion microcells, and irregular distribution of the applied potential [43,44]. Moreover, compared to the true capacitor, the constant phase element (CPE) was used to simulate non-homogeneity double layer capacitance. Meanwhile, the coating layer is also not a homogenous material with containing complex and disorder pathway through the coating layer, which also lead to the heterogeneity of materials [43]. Therefore, the CPE replaced the true capacitor in all equivalent electrical circuit (EEC) models. The following equation (3) with parameters Y, j, ω and n can be mathematically calculated to the result of the impedance of CPE [44].

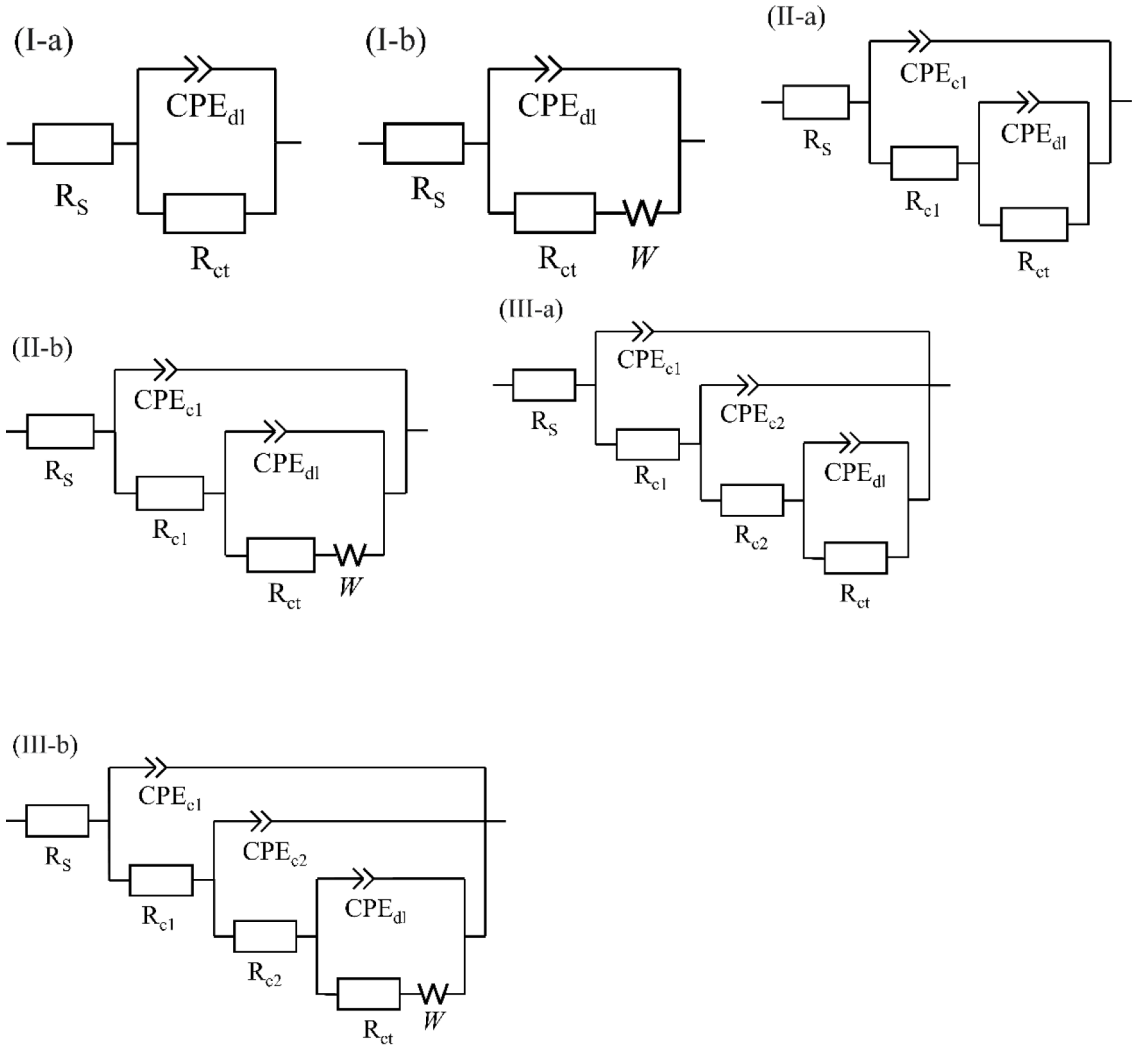


**Fig. 7.** Equivalent electrical circuit (EEC) models.

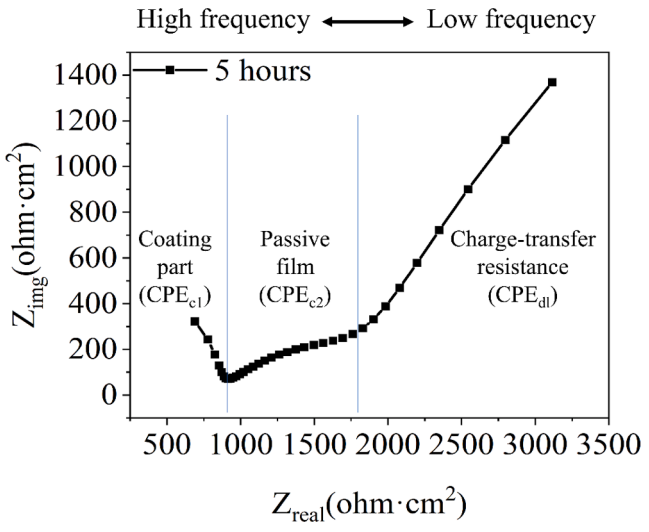


**Fig. 8.** The Nyquist plots of MKPC at 5 h and corresponding constant phase element.

$$Z_{CPE} = Y^{-1} \bullet (j\omega)^{-n} \quad (3)$$

where Y (unit is $\Omega^{-1}\cdot cm^{-2}\cdot s^{n}$) is a constant a phase element and its capacitor is in proportion to the double layer capacitance of a perfect capacitive electrode, n is the control quantity ranging from 0 to 1, $j = \sqrt{-1}$ is the imaginary unit, and the angular frequency of applied alternative current (AC) was represented by ω (ω = 2π*f*, the unit of *f*: Hz). Furthermore, the corresponding effective capacitance was represented by C, and its value was calculated based on the following (4) [45,46]:

$$C = Y^{1/n} \bullet R^{(1-n)/n} \quad (4)$$

where the parameters Y and n are related to CPE and R is its associated parallel resistance, all equivalent electrical circuit elements are shown in Fig. 7.

Fig. 6b and c show the representative evolution of impedance spectra of OPC and MKPC samples within 5376 h (224 days) in 3.5 wt% NaCl corrosion solution in the formation of the Bode (1) to (4) and Nyquist (4) and (5) plots. These specimens were fitted using the equivalent electrical circuit model, EEC-II and EEC- III model shown in Fig. 7II and III, respectively. Like UN specimens, the double layer capacitance also is a part of these two equivalent electrical circuit models, and they were used to illustrate the same functions. But these models are more complicated than EEC-I. The $R_{c1}$ and $CPE_{c1}$ of EEC-II and EEC- III model in Fig. 7 is the resistance of the coating and its corresponding constant phase element; the group of the $R_{c2}$ and $CPE_{c2}$ of EEC- III model represents dielectric properties of passive film; another group's equivalent

electrical circuit elements, $CPE_{dl}$ and $R_{ct}$ is related to the interface properties between the steel to electrolyte or coating layer where corrosion or chemical reaction occurs. The passive layer forming over the substrate steel of MKPC samples will be further discussed by analyzing chemical products measured by XPS, TG/DTA and XRD test. This new chemical product serves as a new passive film to reduce the corrosion rate. As observed from the phase angle-frequency plots shown in Fig. 6(b-1) and (b-2) and Fig. 6(c-1) and (c-2), unlike the UN specimens, the spectrum reveal the two-time constants for the OPC and three time constants for MKPC specimens. For OPC and MKPC samples, the first time constant in high frequency (larger than 10 kHz) shown in Fig. 6 (b-1), (b-2), (b-5) and (b-6) and Fig. 6(c-1), (c-2), (c-5) and (c-6) are attributed to pore resistance and capacitive of the coating part; the second time constant at the middle frequency (1 Hz-10 kHz) is related to the dielectric properties of passive film; the third time constant in the low frequency (smaller than 1 Hz) is associated with double layer capacitance and charger transfer resistance [47–49]. However, in this study, the OPC didn't show the second-time constant related to the dielectric properties of passive film. This is attributed to the curing time being too short to form the protective passive film under high alkali environment. In addition, as indicated from the Fig. 6(b-5) and (b-6), the impedance reduced after the first-time measured data, therefore, it can be related to diffusion processes caused by the presence of corrosion products as illustrated previously. Therefore, the Model II-b will replace the Model II-a to fit the spectra after first time. Meanwhile, as shown in the Fig. 6(b-1) to (b-4), after the 2016 h (84 days), the second-time constant in the bode plots of OPC specimens tends to weak. This is because the coating layer gradually loses its own ability to guard against steel corrosion and the partial degradation of coating layer in the testing solution. Thus, the EEC-II-b was used till the end of the testing period. For MKPC sample, the second time phase tend to weak after the first-time testing, however, as shown in the Fig. 6(c-3) to (c-4), the impedance at the middle frequency (1 Hz-10 kHz) showed some changes in value. Therefore, the EEC model with three time constants were used for MKPC samples. Since the MKPC is also a cementitious material like ordinary Portland cement-based materials, pores, surface cracks and through cracks can form on the coated part during the hydration process and can exist on the hardened magnesium potassium phosphate cement. If these two materials were identical, the impedance of MKCP samples would have decreased as the OPC sample. According to the above hypothesis, the testing results should be as follows: "the coating layer thickness of MKPC sample is lower than coating layer thickness of OPC sample, so, the decreasing rate of impedance of MKPC sample should be lower than the decreasing rate of impedance of OPC sample." However, the actual EIS experimental testing results of MKPC specimens are far better than the OPC specimens. This is the sign of that the anti-corrosion performance of MKPC coating is much better than OPC coating. Based on the Fig. 6(c-4) and (c-6), the impedance started to decrease from the 3360 h (140 days). This could be indicative of corrosion occurring. Therefore, the EEC-III-a model was used to fit the EIS results of MKPC specimens before 3360 h (140 days), and the remaining spectra was fitted by the Model-III-b model with Warburg diffusion impedance. The fitting results were used to analyze the anti-corrosion performance of the magnesium potassium phosphate cement paste coating.

In order to evaluate the anti-corrosion performance, firstly, to compare the trend of impedance shown in the Nyquist plots of OPC and MKPC specimens in Fig. 6b and Fig. 6c. In Nyquist plots, the frequency decreases from the left to the right along the coordinate X-axis. The small arcs in the high frequency range are related to dielectric properties of the coating part and the large arcs at the high frequency range consist of the steel-electrolyte interface where corrosion occurs including the passive layer on the surface of the substate steel [31]. From the first electrochemical test of specimens immersed in corrosion solution for 5 h, the impedance of OPC specimen shown in Fig. 6(b-5) and (b-6) decreases significantly within 1176 h (49 days), then, the impedance value stabilizes until the end of experiment (5376 h) with small reduction. This is because the OPC coating layer starts peeling and forms a significant number of pores, surface cracks and through pathway for water and different ions, so that much more chloride, which is used to convey charged ions in this electrochemical system, penetrates through these flaws to increase the rate of corrosion process. More importantly, this is kind of a vicious cycle process; the rate and degree of corrosion will keep increasing with the larger coating portions or segments peeled from the substrate steel. In addition, any un-hydration particles of cement will then dissolve into the corrosion solution, which also could reduce the integrity of the coating layer to a degree. In the high frequency range of the Nyquist plots, the semi-arc of OPC sample is very hard to be observed. It's also probably because the coating layer thickness is too thin and curing time is too short, which lead to that the coating part was dissolved into corrosion solution. But the properties related OPC coating part can be observed from the Bode plots shown in the Fig. 6(b-1) to (b-4). Moreover, the carbonization of the coating part is also a factor in the change of the impedance, which were discussed in the later part. In contrast, the MKPC coating shows a better anti-corrosion performance. As shown in Fig. 6(c-5) and (c-6), for the first EC test, the maximum impedance value of the MKPC specimen is similar to the first test of OPC specimens. However, over time, the trend of impedance still increased with small fluctuation. It didn't have any significant sign of abating before 3360 h (140 days). The small semi-arc at the high frequency showed the same trend. The magnesium potassium phosphate cement is the fast-setting materials, so the hydration development degree of magnesium potassium phosphate cement in the water cuing condition was affected very little [50]. Combine the results of TG/DTA test shown in the Fig. 18, the resistance of MKPC coating increased with the time, which is partly attributed to anti-carbonization ability. In addition, the larger arc in the high frequency increased with some small fluctuation before 3360 h (140 days), then, it slightly changed and stable until the end of test. For the anti-corrosion ability originated from the passive layer, it was observed from the initial testing at 5 h shown in the Fig. 6(c-1), (c-3) and (c-5). The passive layer state almost was relatively stable according to the frequency range between 1 Hz and 10 kHz shown in the Fig. 6(c-1) to (c-4). It presents the result of the function of passive layer protecting the substrate bars. And the analysis from the Nyquist plots were consistent with the findings from the Bode plots. The real specimens' figures shown in the before and after EC test and the chemical compositions of the products shown in the Figs. 15–20 Based on the previous analysis also confirmed that MKPC has very good anti-corrosion performance and as discussed later in this paper. In summary, the reason why the MKPC coating could provide a far better anti-corrosion performance than OPC is due to two primary reasons based on analyzing the EIS spectrum. One part is due to the stable physical properties of MKPC coating part under the severely corrosive environment. Another is the protective passive layer was formed over the substrate steel.

Based on the previous analysis as shown in the Fig. 7, the corresponding fitted parameters of the equivalent electrical circuit model for UN, OPC and MKPC are tabulated from Table 4 to Table 6, in which $R_p$ and $R_{ct}$ represent the measured evolution of the polarization resistance values and the value obtained from the fitted EIS spectrum, and $R_{coating}$ and $R_{passive}$ are related to $R_{c1}$ and $R_{c2}$. The $R_p$ and $R_{ct}$ are presented in Fig. 9, (a) and (b) are the $R_p$ and $R_{ct}$, respectively. Since the $R_p$ value is contrariwise proportional to the corrosion current, it is normally used to determine the protective ability of coating layer. And, the $R_p$ value can be equal to the $R_{ct}$ only if the testing system is not affected by the diffusion [51].Table 5.

According to the pervious analysis, the $R_{ct}$ was lower than the measured the $R_p$ value due to the accumulation of the iron oxide. To evaluate the transition of steel corrosion from the passive to active state, the threshold values of polarization resistance 0.1-1Mohm·cm$^2$ was used [52]. Similar to the OCP threshold, all three samples didn't reach the requirement of the passive state. As shown in the EIS spectrum, the impedance of the UN and OPC sample reduced from the beginning of the

**Table 4**
The polarization resistance value and experimental fitted data for UN.

| UN (ohm· cm$^2$) | Time (hours) | | | | | | | | | | | | |
|---|---|---|---|---|---|---|---|---|---|---|---|---|---|
| | 5 | 168 | 336 | 504 | 672 | 840 | 1008 | 1176 | 1344 | 2016 | 2688 | 3360 | 4032 | 4704 | 5376 |
| $R_p$ | 2346.108 | 2459.564 | 2718.892 | 2720.918 | 2475.772 | 2552.760 | 2435.252 | 2611.514 | 2378.524 | 1620.800 | 1585.548 | 1506.939 | 1441.296 | 1310.822 | 1191.693 |
| $R_{ct}$ | 2003.714 | 2248.860 | 2471.720 | 2470.421 | 2228.600 | 2350.160 | 2167.820 | 2350.160 | 2066.520 | 1367.550 | 1276.380 | 1209.522 | 1154.820 | 1108.222 | 1031.234 |

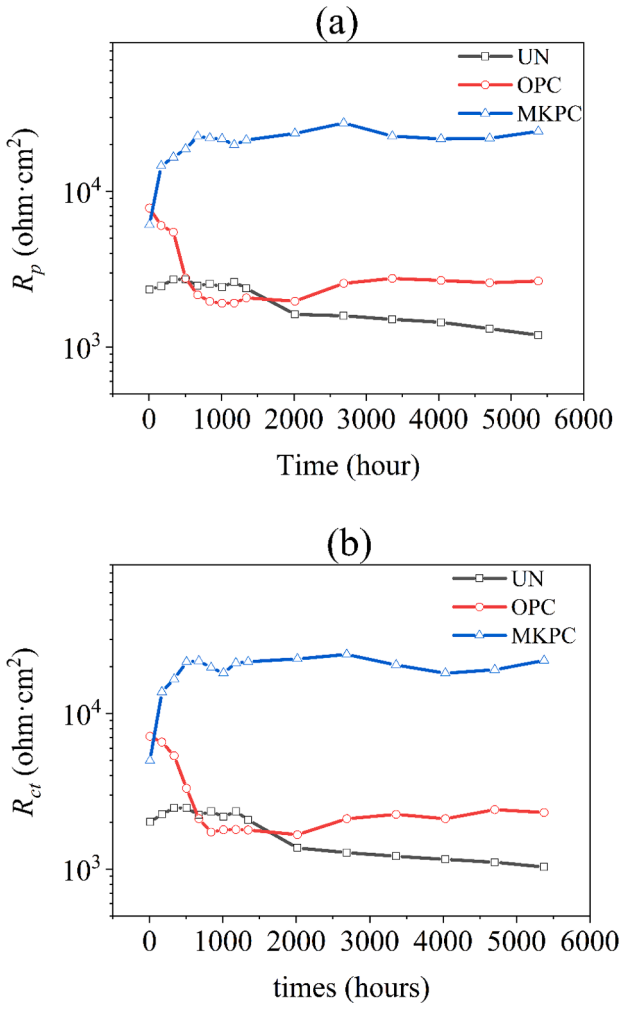


**Fig. 9.** The evolution of polarization resistance and the EIS fitting data (a) $R_p$ and (b) $R_{ct.}$

electrochemical test, the result was entirely predictable. Meanwhile, the $R_p$ value of MKPC sample is also lower than the threshold, yet weren't in good agreement with the reported values from other research [26]. This is believed due to a consideration that the coating layer thickness is too thin. Further work intends to investigate the impact of layer mil thickness. Meanwhile, the trend of UN and OPC samples decreased from the start of test and almost keep stable after 1344 h (56 days). But the $R_p$ value of MKPC sample increased until 672 h (28 days) and slightly fluctuated around its average value over time till to the end of test. Its fluctuation is likely related to the penetration of ions, resulting in the increased charge transfer rate. Under aggressive testing corrosion situation, the stable polarization resistance of MKPC sample demonstrated its good anti-corrosion performance as the evidenced by the fitted $R_{coating}$ and $R_{passive}$ value of MKPC sample presented in Fig. 10. The coating resistance significantly increased in the first week, which is likely attributed to further hardening of un-reacted raw materials. The passive film resistance slightly increased from the beginning of test to the peak value at the time of 1344 h (28 days). This illustrates that the reaction rate between the iron and phosphate radical didn't stop during the EC test as its value kept stable after 1008 h (42 days) with only small reductions. The intact coating layer played an important role in the protection of passive film. In general, even though the polarization resistance of MKPC didn't meet the requirement, it still protected by the both the passive layer and coating part without further significant corrosion.

**Table 5**
The polarization resistance value and experimental fitted data for OPC.

| OPC (ohm· cm$^2$) | Time (hours) | | | | | | | | | | | | |
|---|---|---|---|---|---|---|---|---|---|---|---|---|---|
| | 5 | 168 | 336 | 504 | 672 | 840 | 1008 | 1176 | 1344 | 2016 | 2688 | 3360 | 4032 | 4704 | 5376 |
| $R_p$ | 7818.336 | 6030.703 | 5469.113 | 2772.049 | 2160.867 | 1964.072 | 1910.648 | 1915.900 | 2066.557 | 1969.762 | 2565.929 | 2757.386 | 2676.346 | 2587.202 | 2652.034 |
| $R_{ct}$ | 7131.52 | 6543.98 | 5348.64 | 3302.38 | 2107.04 | 1730.204 | 1788.958 | 1795.036 | 1782.88 | 1665.372 | 2107.04 | 2248.86 | 2107.04 | 2410.94 | 2309.64 |

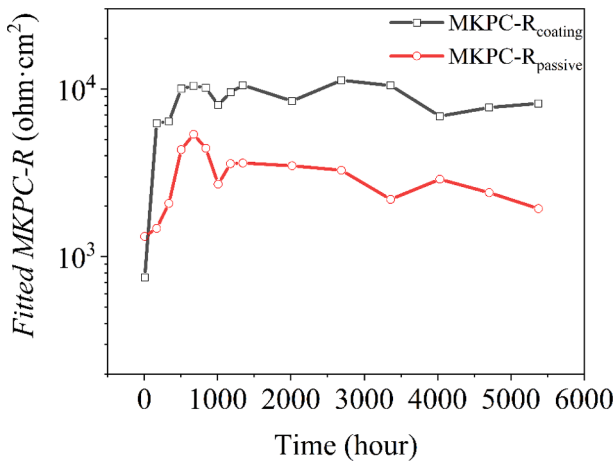


**Fig. 10.** The fitting data of MKPC: $R_{coating}$ and $R_{passive}$.

### 3.3. Potentiodynamic polarization (PDP)

Fig. 11 presents the potentiodynamic polarization (PDP) plots of the OPC and MKPC specimens immersed into 3.5 wt% NaCl solution for 5 h, 1344 h (56 days) and 5376 h (224 days). Table 7 shows the values of corrosion current density ($I_{corr}$) and corrosion potential ($E_{corr}$) which

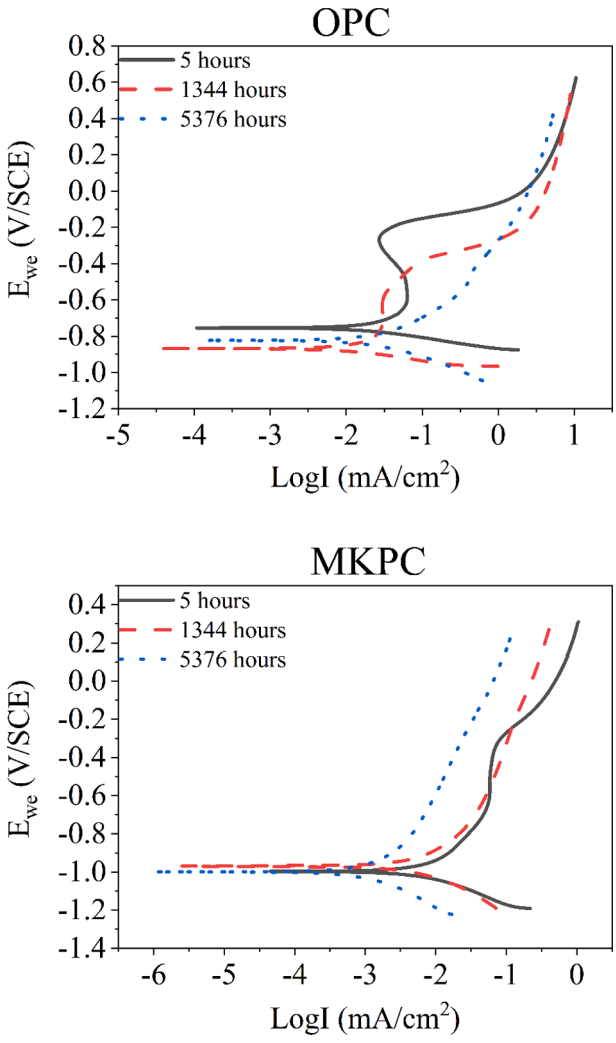


**Fig. 11.** Potentiodynamic polarization curves for OPC and MKPC specimens.

**Table 6**
The polarization resistance value and experimental fitted data for MKPC.

| MKPC ($ohm \cdot cm^2$) | Time (hours) 5 | 168 | 336 | 504 | 672 | 840 | 1008 | 1176 | 1344 | 2016 | 2688 | 3360 | 4032 | 4704 | 5376 |
|---|---|---|---|---|---|---|---|---|---|---|---|---|---|---|---|
| $R_p$ | 6104.338 | 14595.304 | 16572.680 | 18726.318 | 22630.420 | 22022.620 | 21779.500 | 19903.576 | 21394.560 | 23562.380 | 27500.080 | 22650.680 | 21738.980 | 21941.580 | 24312.000 |
| $R_{ct}$ | 4983.961 | 13756.543 | 16633.460 | 21495.860 | 21799.764 | 19692.727 | 18213.741 | 21131.180 | 21556.646 | 22448.080 | 23987.840 | 20503.122 | 18152.962 | 19105.180 | 21921.325 |
| $R_{coating}$ | 750.4304 | 6258.314 | 6406.212 | 10022.622 | 10450.108 | 10166.468 | 8004.726 | 9532.33 | 10543.304 | 8462.602 | 11254.43 | 10482.524 | 6884.348 | 7755.528 | 8201.248 |
| $R_{passive}$ | 1320.749 | 1475.131 | 2078.676 | 4349.822 | 5356.744 | 4430.862 | 2706.736 | 3588.046 | 3616.410 | 3484.720 | 3276.042 | 2198.210 | 2893.128 | 2410.940 | 1933.209 |

**Table 7**
Parameters extracted from potentiodynamic polarization curves for OPC and MKPC specimens.

| Time (hours) | Ecorr (mV/SCE) | | Icorr ($\mu A/cm^2$) | | Corrosion rate (mm/year) | |
|---|---|---|---|---|---|---|
| | OPC | MKPC | OPC | MKPC | OPC | MKPC |
| 5 | −868.568 | −997.484 | 14.763 | 7.903 | 0.17128 | 0.09169 |
| 1344 | −953.089 | −969.436 | 27.453 | 5.971 | 0.31851 | 0.06928 |
| 5376 | −825.883 | −999.615 | 27.051 | 2.051 | 0.31385 | 0.02379 |

were extracted from potentiodynamic polarization plots, and the corrosion rate (CR) was calculated based on (5) [53]:

$$CR = \frac{I_c \bullet K \bullet EW}{d \bullet A} \tag{5}$$

where CR is corrosion rate, $I_c$ is the corrosion current in Ampere, K is the constant that defines the units of the corrosion rate, EW is equivalent weight (in g/equivalent), d is the density, and A is the sample area.

For the value of both the OPC and MKPC specimens, the threshold of corrosion current density, 0.5 $\mu A \cdot cm^{-2}$ [8,54], were exceeded, which is an indication of active corrosion. The corrosion current density of OPC specimens and MKPC specimens however presented quite different trends. The OPC increased from the first test until the end of test. On the other hand, the current density value of MKPC sample gradually decreases, since the OPC coating layer loses its protection ability and became weaker with the increasing corrosion degree. For the MKPC specimens, except for the factor of intact coating layer, the progress of coating layer and new passive layer over the reinforcement surface should be the critical factors for anti-corrosion performance under all other conditions unchanged. In addition, the corrosion rate and current density, which reduced from 0.09169 to 0.02379 mm ($3.6098e^{-3}$ to $9.3661e^{-3}$ in) per year and 7.903 to 2.051 $\mu A/cm^2$, conform to the previous discussion from analysis of EIS test.

In summary, according to the three parts of electrochemical test, the magnesium phosphate cement paste coating exhibits a far better corrosion protection ability than OPC coating in the same testing environment. Even though the active state threshold of open-circuit potential value, polarization resistance and corrosion current density of MKPC sample were exceed, the relatively stable open-circuit potential value, increased polarization resistance, and corrosion current density and corrosion rate reducing with the time elapsed proved that the magnesium potassium phosphate cement paste coating could protect the bars. Another important factor influenced the results is the thickness of coating layer. It is believed that the anti-corrosion ability could be improve by increasing the coating layer thickness. The following section will go a step further in this study to explain the protection mechanism of magnesium phosphate cement coating.

### 3.4. Visual inspection

Fig. 12 shows the corrosion maps of three sample types, which were immersed into 3.5 wt% NaCl corrosion solution and tested under the same indoor environment, after the 5376 h (224 days) electrochemical test. In these figures, the degree of corrosion trends to become weak from the samples without coating compared to the samples with ordinary Portland cement coating, and lastly, to the samples with magnesium potassium phosphate cement paste coating.

In Fig. 12(a-1) and (b-1), the bottom of beaker has a large amount of dark yellow sediment deposits due to corrosion. In the UN bare bar's beaker, it is believed that there are black ($Fe(OH)_2$) and red ($Fe_2O_3$) rust. In the OPC sample's beaker, besides rust, the sediment also contains some peeled coating portions. The substrate steel volume increased due to the process of forming the iron oxide, which leads to the rust and compromising/breaking down bursting the coating layer. Fig. 12(b-2) indicates some coating portions were peeled, and the substrate steel has


**Fig. 12.** Bar surface conditions (number1: test condition, number2: samples without any treatment and number 3: samples with peeling off the coating) of samples after 5376 h EC test for:(a) UN, (b) OPC and (c) MKPC.

been exposed directly to the electrolyte, which increases the rate of transferring electron; this process ultimately leads to an increased corrosion rate. As expected, after removing the coating layer, the surface of steel is full of the dark rust as shown in Fig. 12(b-3). In contrast, the beaker of samples with MKPC coating shown in Fig. 12c only had very minor sediment. The sample surface remained intact except for a few very minor corrosion spots on its surface. Most importantly, after peeling the coating layer, the substrate steel presents a white layer over the entire surface, which is consistent with the steel's original dark gray color. According to the discussion above, the effect in preventing corrosion of bars using magnesium potassium phosphate cement paste coating seems more pronounced than using OPC coating. And the anti-corrosion performance of MKPC specimens is partly attributed to a passive film.

Meanwhile, the coating parts of the OPC and MKPC samples were observed through a microscope as shown in the Fig. 13a and Fig. 13b show the coating part pattern of the OPC and MKPC samples, respectively. The 7 days curing of ordinary Portland cement paste shows a few pore defects over it compared with the 7 days curing of MKPC paste, as shown in Fig. 13(b-1). In addition, the red circle in Fig. 13(b-1) shows some crystal particle, which is assumed the efflorescence formed due to the low M/P ratio. The nature of efflorescence has a very negative influence on the strength and volume stability of materials performance and has not been well investigated yet [55]. So, the anti-corrosion performance may be improved by preventing the formation of efflorescence. The formation of transferring electron pathway is usually initiated from these weak regions. Furthermore, as indicated in Fig. 13 (a-2) and Fig. 13(a-3), a larger amount of rust generated by substrate steel was attached over the inner surface of OPC samples, and some through crack was observed on its surface. Furthermore, the inner rust has passed through a weaker region of the coating layer, and is visible on its outer surface. On the other hand, even though the corrosion spot also is observed on the inner surface of MKPC coating layer shown in the Fig. 13(b-2), it is far slighter than the OPC samples. Meanwhile, the outer surface's corrosion spot of MKPC samples shown in Fig. 13(b-3) are also smaller and lighter than OPC samples, and the outer surface showed no significant through crack. These signs showed the hardened magnesium potassium phosphate cement paste coating has lots of outstanding features, especially the low permeability and high durability [17–19], which was considered to be a good protective material for delaying the steel corrosion process and rate. In summary, the results of morphology of the real samples after 5376 h (224 days) EC test are in consistent with the results and analysis from the previous electrochemical tests in this study for uncoated or coated specimens.

The above referenced EC test and observation of corrosion samples proved that the magnesium potassium phosphate cement paste coating exhibited good anti-corrosion behavior. An investigation of transition zone characteristics between the steel substrate and magnesium potassium phosphate cement paste coating further explains this result. Fig. 14 indicates the typical Secondary electrons (SE) and element maps of cross-section morphologies 7 days cured MKPC sample. Distinctive features of microstructure and the distribution of the characteristic elements of substrate steel and magnesium potassium phosphate paste coating layer reveal a clear interface. The steel part is comparatively smooth and flat, which is shown at the bottom of the Fig. 14. Additionally, the top part of the SE image corresponds to the magnesium potassium phosphate paste coating part, which is mainly composed of hardened magnesium potassium phosphate paste, un-hydrated magnesium particles and phosphorus and potassium elements.

Even though the magnesium potassium phosphate is a fast-setting material, the coating could exhibit increased anti-corrosion ability with the further hydration of these un-hydrated raw materials. This finding confirmed the previous analysis of electrochemical testing data shown in the Fig. 6(c-5) and (c-6) and how the small semi-arc in the high frequency kept increasing with some fluctuation. The coating parts has little cracks through the cross-section and no significant micro pores in coating area, which provide good density, which reduces the charged ions passing through the coating layer and thereby reduces

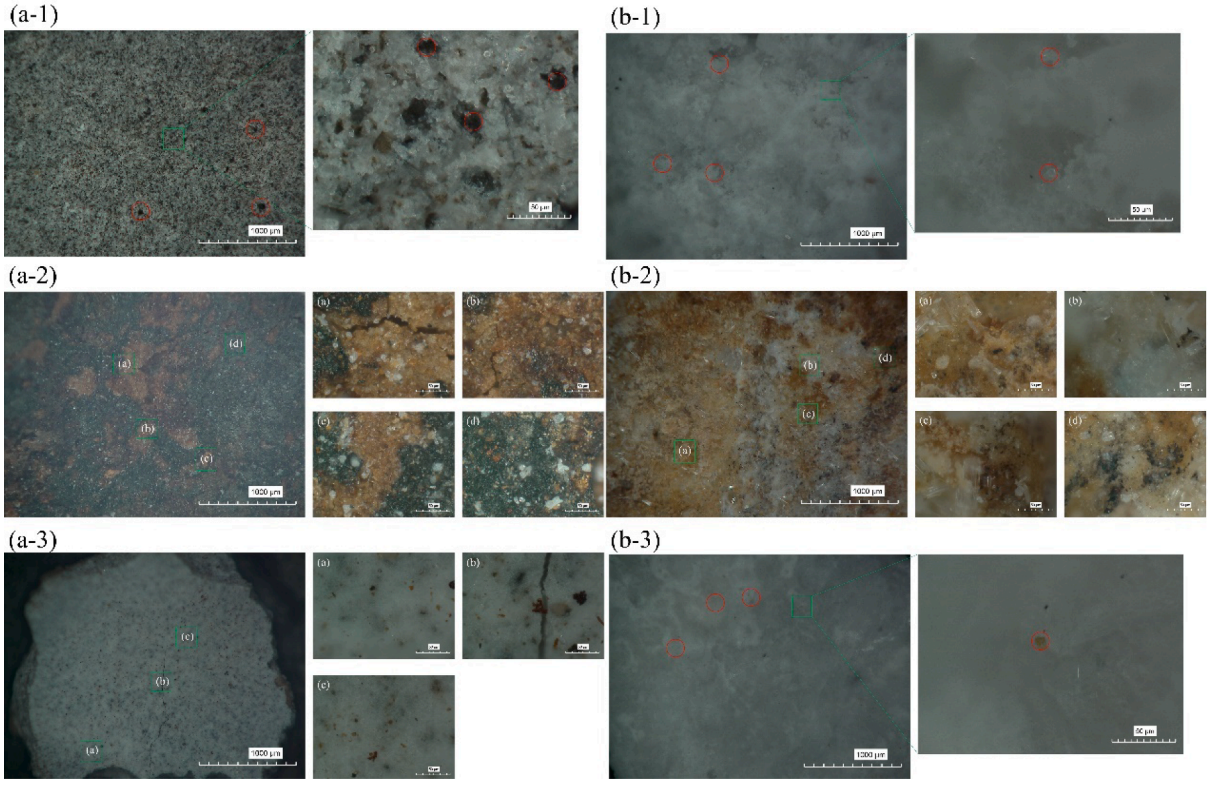


**Fig. 13.** Coating surface conditions (number1: samples for curing 7 days before EC test, number2 and 3: inner and outer surface of coating part after 5376 h EC test) of samples for:(a) OPC and (b) MKPC.

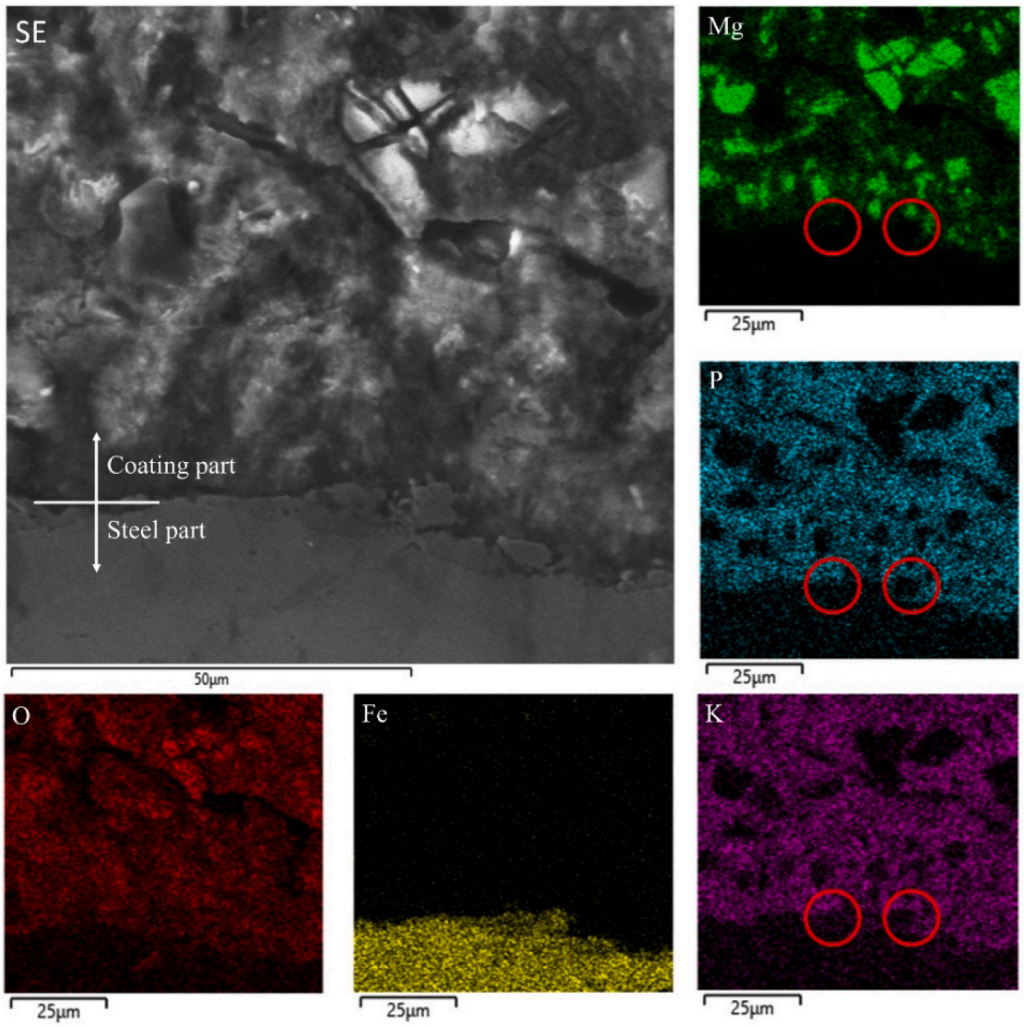


**Fig. 14.** The scanning electron microscope of cross-section of MKPC sample before the EC test for: (SE) typical Secondary electrons image, (O)oxygen, (Fe) iron, (K) potassium, (P) phosphorus and (Mg)Magnesium.

opportunities of exchanging electrons between the iron ions and other ions. These observations are consistent with EC test's data presented previously. As expected, this desired density could reduce the corrosion rate, so that to increase its protective ability for bars. Even though the MKPC materials have a very good bond ability with steel, after polishing the surface, a small gap is visible. As discussed above, the protective passive film formed before the electrochemical test, thus, to focus on observing the changes of the three chemical elements, magnesium (Mg), phosphorus (P) and potassium (K), is the key factor to locate the passive layer. It's not hard to observe that the area closing to the substrate steel appeared larger amount of phosphorus elements than other two elements, which could be inspected in the red circle zone of Fig. 14(Mg), (P) and (K). And this finding matched the following XPS and XRD testing data. The formed protective passive layer is the iron phosphate compound. More detailed analysis of this passive layer is presented in the following discussion.

### 3.5. X-ray photoelectron spectroscopy (XPS) analysis

The XPS spectra of MKPC samples before and after the 5376 h (224 days) EC test shown in Fig. 15 and Fig. 16 indicate the change of the Binding Energy (BE) value of three measured elements: oxygen, iron, and phosphorus. The calibration value C 1 s peak (284.6 eV) shown in Fig. 15(a) and Fig. 16(a) were applied on both of the two measured XPS spectrum. Meanwhile, the BE value of all elements and their chemical group are referred to using the published paper and are shown in Table 8 [56–65]. As shown in the Fig. 15(b), the O 1 s peak were deconvoluted into three components. The peaks at 529.7 eV, 531.4 eV and 531.9 eV were attributed to the $OH^{-}$, $PO_4^{3-}$ and $O^{2-}$, respectively. Additionally, the binding energy for Fe and its compounds are present in the measured data, which could be assigned to $Fe^0$, Fe(II) species, Fe(III) species and its Fe(II) satellite peak. Its corresponding BE value was presented in Table 8 Fe $2p_{3/2}$. In terms of phosphorus, the deconvoluted P 2p spectra exhibit two peaks which could be assigned to $H_2PO_4^-$ (BE = 132.6) and $PO_4^{3-}$ (BE = 133.8).

For the samples cuing 7 days, when to coat the MKPC paste over the surface of steel bar, the bar was under the moist environment with oxygen, so, some chemical reaction may have already occurred on the surface of bar before the EC test. And the polished process could not guarantee remove all the compounds of iron and oxygen. During the seven days curing time, therefore, the surface of steel bar contained Fe (II) species, Fe(III) species besides the $Fe^0$. At the same time, after the iron lost two electrons, the iron reacted with phosphate to form Fe $(H_2PO_4)^-$. Based on research by Wagh [36], the chemical process of iron under a phosphate environment presence is summarized as (6):

$$Fe^{2+} + 2H_2PO_4^- \rightarrow Fe(H_2PO_4)^- \quad (6)$$

As shown in Fig. 15 and Fig. 16, there are some differences between the measured spectrum before and after the electrochemical testing, which are the chemical group of iron and phosphorus. For the corrosion

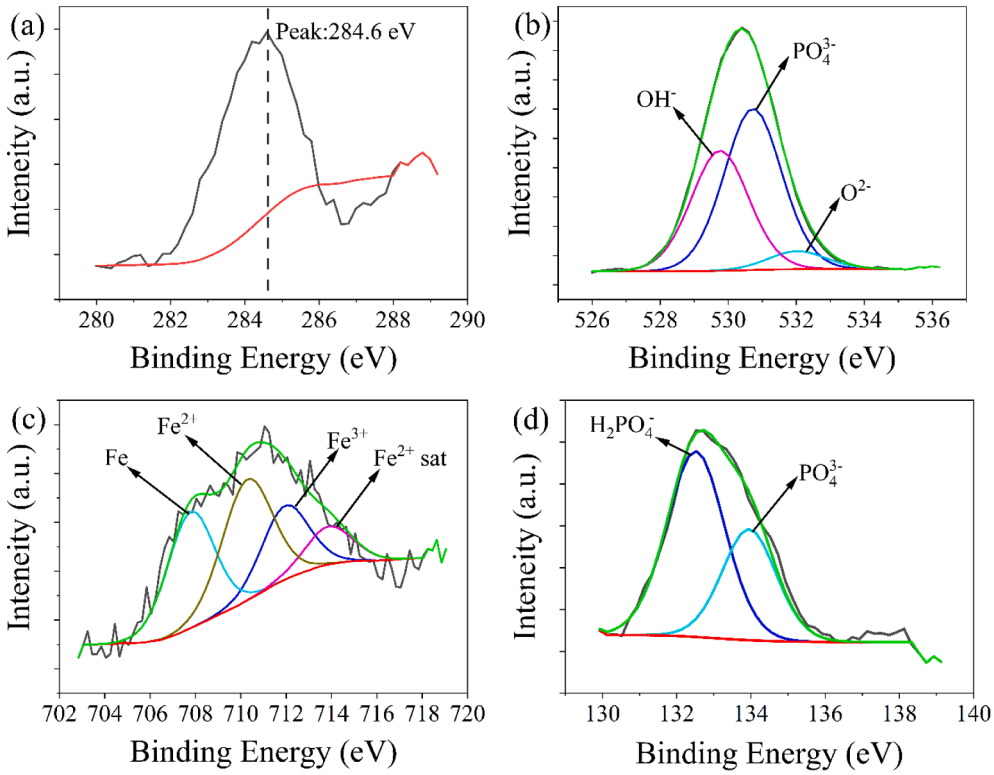


**Fig. 15.** High-resolution X-ray photoelectron spectrum of MKPC samples before the EC test for: (a)C 1 s, (b)O 1 s, (C)Fe 2p and (d)P 2p.

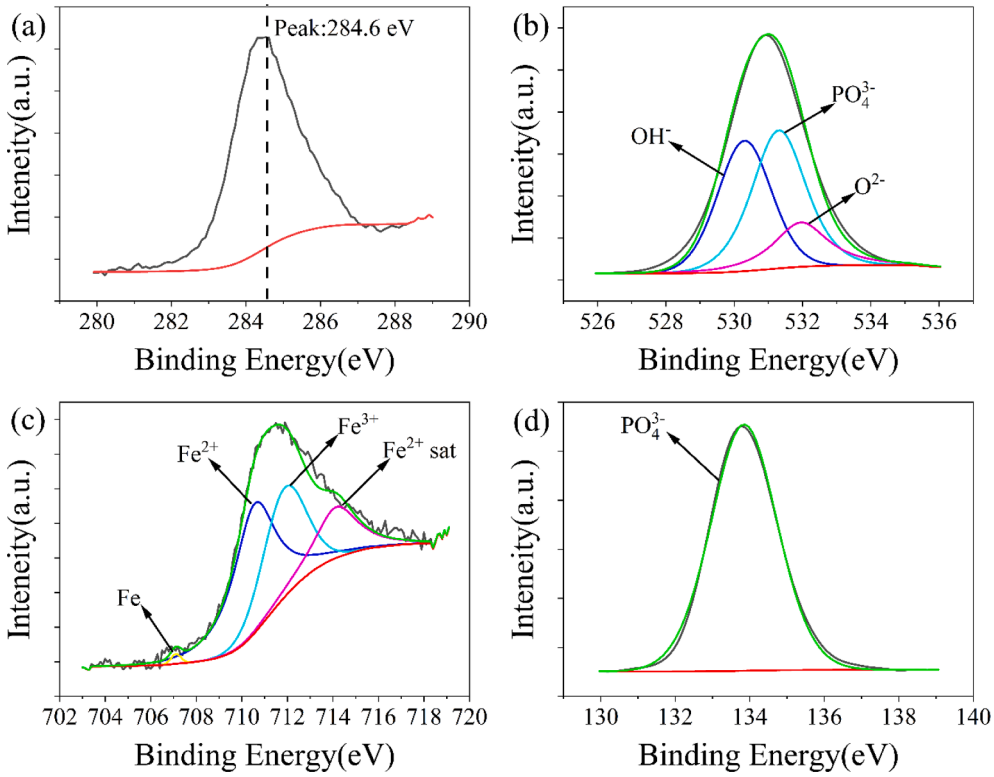


**Fig. 16.** High-resolution X-ray photoelectron spectrum of MKPC samples after the 5376 h EC test for: (a)C 1 s, (b)O 1 s, (C)Fe 2p and (d)P 2p.

solution with OPC sample, the pH value was changing from around 11.6 at first 672 h (28 days) to around 9.2 at the end of the test. Meanwhile, the testing solution was directly exposed to an indoor laboratory environment [temperature is 20 ± 2 ℃ (64 to 72 °F) and air humidity is 55 ± 20 %] without any barrier. Therefore, the oxygen in the air was dissolved into the corrosion solution and engaged in the process of steel corrosion reactions [28]. Under the severe corrosion testing

**Table 8**
Estimated XPS peak positions of elements on the surface of substrate steel bar.

| Peak | Component | Binding energy/eV | Reference |
|---|---|---|---|
| C 1 s | C | 284.6 | [62] |
| O 1 s | $OH^{1-}$ | 529.7 | [60] |
| | $OH^{1-}$ | 530.1 | [64] |
| | $O^{2-}$ | 531.9 | [59] |
| | $PO_4^{3-}$ | 531.4 | [56] |
| Fe $2p_{3/2}$ | $Fe^0$ | 707.3 | [63] |
| | $Fe^{2+}$ | 709.6 | [61] |
| | $Fe^{3+}$ | 711.4 | [65] |
| | $Fe^{2+}$satellite | 714.0 | [57] |
| P 2p | $H_2PO_4^{1-}$ | 132.6 | [58] |
| | $PO_4^{3-}$ | 133.8 | [56] |

environment, the oxygen gradually dissolved into the corrosion solution, and reacted with the iron, which lead to the formation more black rust ($Fe(OH)_2$) and red rust ($Fe_2O_3$). The chemical reaction process can be summarized as (7) and (8):

$$Fe^{2+} + 2OH^- \rightarrow Fe(OH)_2 \quad (7)$$

and

$$4Fe(OH)_2 + O_2 \rightarrow 2Fe_2O_3 + 4H_2O \quad (8)$$

In addition, with the presence of the water, oxygen and ions increasing by passing the coating layer, the surface of substrate steel underwent the chemical reaction (7) to (12) lasting 5376 h (224 days) without stop, so that the surface's iron element was hard to be detected by radiation. This is because the counts of measured spectra and the depth of an element atom to the surface are in the inverse proportion. It means the closer to the surface an element atom, the more contribution to the spectra it yields. Thus, the surface chemical group are primarily composed by the Fe(II) and Fe(III) species. Meanwhile, the related phosphate radical was provided by the soluble phosphate dissolving process as shown in equation (9) to (11):

$$KH_2PO_4(aq) \leftrightarrow H_2PO_4^-(aq) + K^+(aq) \quad (9)$$

$$H_2PO_4^-(aq) \leftrightarrow HPO_4^{2-}(aq) + H^+(aq) \quad (10)$$

and

$$HPO_4^{2-}(aq) \leftrightarrow PO_4^{3-}(aq) + H^+(aq) \quad (11)$$

Furthermore, as shown in the Fig. 15d, the $PO_4^{3-}$ (not the principal compounds) was formed and is represented as *(12) to (14)* [36]:

$$4Fe(OH)_2 + O_2 + H_2O \rightarrow 4Fe(OH)_3 \quad (12)$$

$$Fe(OH)^{2+} + 2H_2PO_4^- \rightarrow FeH(HPO_4)_2 + H_2O \quad (13)$$

and

$$Fe(OH)^{2+} + 2HPO_4^{2-} \rightarrow FePO_4 + H_2O \quad (14)$$

Then, the chemical processes from (12) to (14) were also involved in reacting at same time. Finally, the chemical products, $Fe(III)PO_4$, was produced. Therefore, as shown in Fig. 16d, the phosphorus spectra only contains the $PO_4^{3-}$. Meanwhile, due to the long-term reactions as the surface of substrate steel, the spectrum indicates almost all substrate steel surface $Fe^0$ had lost electrons and changed into new chemical compounds as discussed above. Based on the analysis and measured data by XPS test, beside the rust, the new formed chemical compound on the steel surface due to the substrate steel reacting with magnesium potassium phosphate cement was dominated by $Fe(III)PO_4$.

The pH value of corrosion solution with MKPC samples was always under the 9. Based on previous research [26], it showed that the pH value of MKPC at the initial stage is usually lower than 7. In civil engineering applications, the protective passive layer of steel must be at a pH value above 10.5 to prevent corrosion [27]. Thus, the passive film formed due to the high pH value doesn't contribute to the anti-corrosion ability of magnesium potassium phosphate cement coating.

In summary, this process was divided into two components, one relating to oxidation of iron, the another focusing on the chemical reaction between the iron oxide and phosphate to form a new chemical products, $Fe(III)PO_4$. At the stage for MKPC samples curing at 7 days and after the EC test, the previous chemical reaction occurred on the surface of the substrate steel. The measured chemical group data from the XPS test shown in Fig. 15 and Fig. 16 confirmed these analysis and chemical reaction process.

### *3.6. Chemical composition of coating part by X-ray diffraction (XRD) analysis and thermogravimetric/differential thermal analysis (TG/DTA)*

The chemical products decomposition temperature of the OPC and MKPC samples' coating part during the TG/DTA test is recorded and shown in Fig. 17 and Fig. 18, respectively. These figures show the TG/DTA spectra of OPC and MKPC samples before and after the 5376 h (32 weeks) EC test. For OPC samples after the 5376 h (32 weeks) EC test, two major weight loss are observed on the Fig. 17.

The first loss weight peak was located at approximate 30–300 ℃ (86–572 °F), which is attributed to the formation of calcium silicate hydrate (C—S—H), AFt and AFm phases [66]. When the temperature reaches around 680 ℃ (1256 °F), second peak was measured, which indicates the presence of $CaCO_3$. Compared with the OPC samples before EC test, there are three main differences. One is rate of content weight at the peak of approximate 100 ℃ (212 °F); this is because the degree of hydration is different, the longer hydration time means the more hydration products. Secondly, for the OPC sample before EC test, one more weight loss peak at around 450 ℃ (842 °F) is observed, indicting the presence of $Ca(OH)_2$. But after the 32 weeks EC test, this weight losing peak disappeared. In the meantime, the third difference is the content weight of $CaCO_3$ increased significantly. The carbon dioxide ($CO_2$) was dissolved into the solution to lead to corrosion, commonly referred to as "carbonation induced corrosion" [29]This process of OPC samples is represented by the following *(15)*:

$$Ca(OH)_2 + CO_2 \rightarrow CaCO_3 + H_2O \quad (15)$$

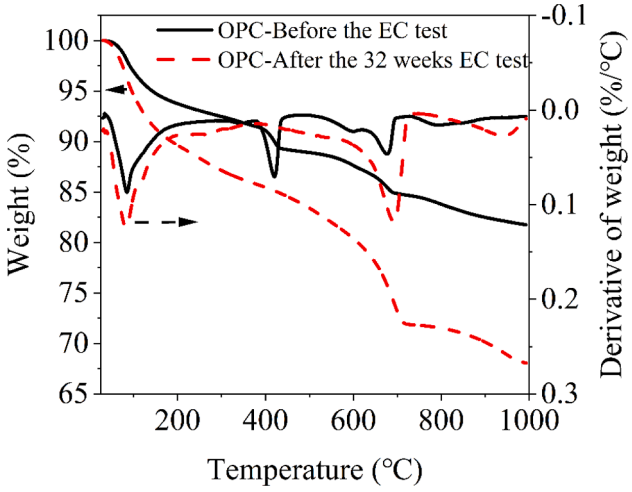


**Fig. 17.** TG/DTA of OPC samples for black line: OPC before the EC test, and red line: OPC after the 5376 h (32 weeks) EC test. (For interpretation of the references to color in this figure legend, the reader is referred to the web version of this article.)

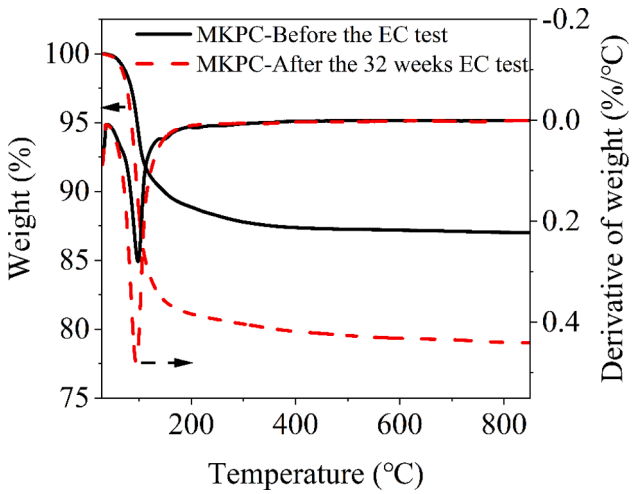


**Fig. 18.** TG/DTA of MKPC samples for black line: MKPC before the EC test, and red line: MKPC after the 5376 h (32 weeks) EC test. (For interpretation of the references to color in this figure legend, the reader is referred to the web version of this article.)

In general, during the 32 weeks EC test, severe carbonization occurred for the OPC samples. Carbonation-induced corrosion was also considered as a type of reinforcement corrosion, which also leads to a volume increase of substrate reinforcement [67]. Therefore, besides the peeled coating portion of OPC sample, the severe carbonization is also a main factor, which led to the deterioration of anti-corrosion performance of the ordinary Portland cement paste coating. This finding verifies the previous electrochemical testing conclusions yet again.

For MKPC samples, only one decomposition peak was measured as shown in Fig. 18. The peak of the sample after 32 weeks EC test is higher than seven days cured sample. This is because the testing time should be counted for curing time. The longer curing time, the more hydration products. Based on the thermogravimetric analysis, the main product of magnesium phosphate cement is decomposed starting at around 60 ℃ (140 °F) and almost complete at around 200 ℃ (392 °F) [16]. The decomposition of MKPC can be written as the following equation *(16)*:

$$MgKPO_4{\cdot}6H_2O \xrightarrow{60-200^\circ C(140-392^\circ F)} MgO + KPO_3 + 6H_2O \quad (16)$$

Above 200 ℃ (392 °F), the derivative of weight of the MKPC sample trended to zero and the trend of these two samples were the same, which means the chemical compositions of MKPC sample do not change much during the 5376 h (32 weeks) EC test. In addition, the severe carbonization was not found in the coating part of MKPC sample. This factor also emphasizes the reason for maintaining the stability of the anti-corrosion performance of MKPC paste. The thermal decomposition degree of the Iron(III) phosphate is around 158–180 ℃ (316.4–356 °F). The Iron(III) phosphate was not detected is likely due to the small amount in the treated coating layer.

Generally speaking, part of corrosion resistance enduring ability was affected by whether the coating layer was partially or fully carbonized or not. Moreover, the MKPC coating exhibits a good carbonatation resistance performance and relatively stable chemical properties.

To further determine the chemical compounds after analyzing TG/DTA data, the coating part of OPC and MKPC samples before and after the 5376 h (32 weeks) EC test were qualitatively analyzed by the XRD test and the diffraction patterns are shown in Fig. 19 and Fig. 20.

All elements and their compounds are displayed in Fig. 19 and Fig. 20, and the position of peaks are referred to using the published paper and are shown in Table 9. For the OPC sample spectra after the 5376 h (32 weeks) EC test, one of the main hydration products, calcium hydroxide, were consumed by the carbon dioxide due to the chemical reaction shown in (15). Meanwhile, besides the calcium carbonate, no other significant peak was observed. It means that this measured coating part of OPC sample after EC test has almost been completely carbonized. Even though this one testing particle cannot represent the whole entire

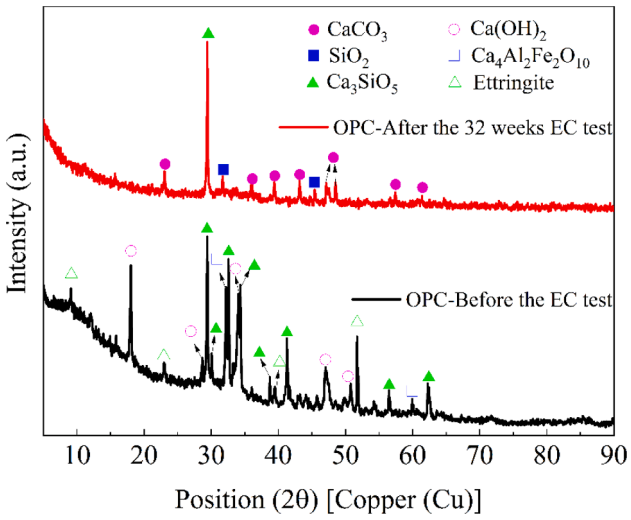


**Fig. 19.** XRD pattern of OPC sample for black line at the bottom: OPC before the EC test, and red line at the top: OPC after the 5376 h (32 weeks) EC test. (For interpretation of the references to color in this figure legend, the reader is referred to the web version of this article.)

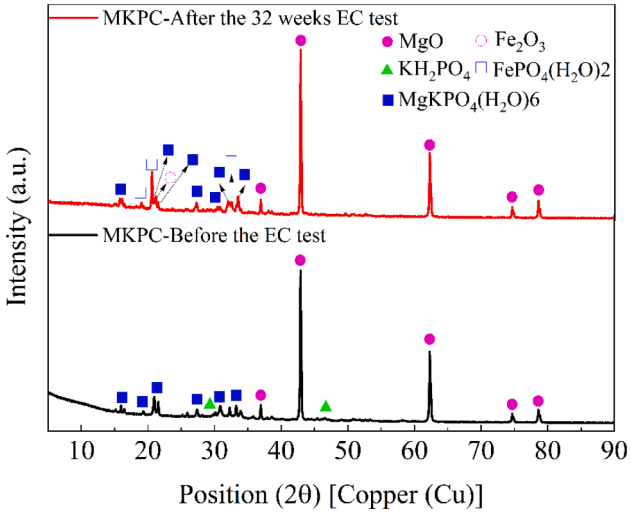


**Fig. 20.** XRD pattern of MKPC sample for black line at the bottom: MKPC before the EC test, and red line at the top: MKPC after the 5376 h (32 weeks) EC test. (For interpretation of the references to color in this figure legend, the reader is referred to the web version of this article.)

**Table 9**
Estimated XRD peak positions of elements for coating paste.

| typical | Molecular formula | Reference |
|---|---|---|
| Magnesium oxide | MgO | [69] |
| Iron (III) oxide | $Fe_2O_3$ | [70] |
| Magnesium potassium orthophosphate hydrate | $MgKPO_4{\cdot}6(H_2O)$ | [71] |
| Potassium hydrogen phosphate | $KH_2PO_4$ | [72] |
| Iron (III) phosphate hydrate | $FePO_4{\cdot}2(H_2O)$ | [73] |
| Calcium carbonate | $CaCO_3$ | [74] |
| Calcium silicate | $Ca_3SiO_5$ | [75] |
| Calcium hydroxide | $Ca(OH)_2$ | [76] |
| Calcium aluminum iron oxide | $Ca_4Al_2Fe_2O_{10}$ | [77] |
| Ettringite, syn | $Ca_6Al_2(SO_4)_3(OH)_{12}{\cdot}25(H_2O)$ | [78] |

coating layer, it still proves that the OPC's chemical products was changed due to serious carbonation. On the other hand, the presence of calcium hydroxide, ettringite and some un-hydrated cement particles are the major phases for the OPC sample before EC test, and its chemical composition is more complicated than the OPC samples after EC test. This is because, at the early stage, along with the hydration, the new chemical products were produced, but at the seven days cured time, un-hydrated raw materials are still in there [68].

For the MKPC sample, the peaks representing magnesium potassium orthophosphate hydrate ($MgKPO_4{\cdot}6(H_2O)$), un-hydrated Magnesium oxide (MgO) and Potassium hydrogen phosphate ($KH_2PO_4$) were easily identified in the XRD pattern of the MKPC paste cured for 7 days. In addition, in the visual inspection part, the microstructure properties and cross section map of the coating part corresponded to this diffraction pattern. However, the ferric iron compound was not detected by the radiation on the samples before EC test, this is probably because, at the initial hydration stage, the amount of formed iron compound was very small, and it only appeared on the surface of substrate steel. Compared to the MKPC samples before and after the 5376 h (32 weeks) EC test, the main difference is that Iron (III) oxide ($Fe_2O_3$) and Iron (III) phosphate hydrate ($FePO_4{\cdot}2(H_2O)$) were detected. This is because substrate steel reacts with the magnesium potassium phosphate cement paste and a large amount of iron is oxidized. Thus, the ferric iron compound peak was emerged on the XRD pattern. More importantly, Iron (III) phosphate was detected. These findings are in accord with the analysis from the XPS pattern of the substrate steel surface and its formation process as presented in equation (6) to (14). In summary, the XPS and TG/DTA pattern and analysis as presented above are corroborated by the XRD results.

## 4. Conclusion

This study was developed to investigate and evaluate the steel bar anti-corrosion performance under the protection of the ordinary Portland cement paste and magnesium phosphate cement paste coating referred to as OPC and MKPC, respectively in this work. Through a thorough comparison and discussion of two types coating in the electrochemical properties, visual inspection and chemical composition between before the electrochemical test and after the 5376 h electrochemical test, the following conclusion are summarized:

For 5376 h impedance developing process of the magnesium potassium phosphate cement paste coating, unlike the OPC paste coating-decreasing around 64 % from the first test, the MKPC kept increasing until the 3369 h (140 days) and maintained stability to the end of test in the corrosive environment-increasing around 7 times from the first test, supporting that the MKPC coating paste developed a far better excellent anti-corrosion performance than OPC coating. Therefore, this material may be considered to be practical for some underwater construction and some traditional reinforcement concrete structures to reduce the corrosion rate and to eventually extend service life of the structure.

The measured polarization resistance value and corrosion current density of the MKPC samples didn't meet the threshold level. However, the OCP at around −0.87 and polarization resistance value at around $2E10^4$ were remained stable during a large part of electrochemical test, and the corrosion current density tended to decrease around 75 % during the whole 5376 h EC test. Combined with the MKPC samples' integral coating without flaws after 5376 h (224 days), the magnesium potassium phosphate cement paste coating displayed strong robust properties to delay the corrosion rate.

The chemical composition of the OPC sample after the 5376 h EC test was dominated by C—S—H and calcium carbonate and instead of C—S—H and calcium hydroxide. That is to say, the OPC sample at the long-term EC test resulted in severe carbonization. On the other hand, under the same testing environment, there was no significant difference between the MKPC sample's chemical compositions before and after the EC test. This means that the carbonation resistance of MKPC coating for decreasing the corrosion rate is far better than the OPC coating.

The coating part of MKPC sample remained an intact surface without exposing the substrate steel to the corrosion solution during the 5376 h EC test, but the OPC sample's coating part peeled due to corrosion and other related reasons. Obviously, the measured data of the EC test of the OPC sample showed that its anti-corrosion protection continued to decrease around 45 % throughout the EC test based on the corrosion current density. On the other hand, based on the analysis of the TG/DTA and XRD test, the chemical compositions of the MKPC coating layer didn't indicate significant changes. Therefore, the more stable chemical composition of MKPC sample reflects that its chemic and physical characteristic was more stable.

According to an analysis of the measured data of XPS, TG/DTA and XRD, the electron exchange appeared on the surface of the substrate steel of MKPC sample at the initial EC test, which indicates that corrosion is occurring at this time. Furthermore, a new product, iron (III) phosphate, was detected at the substrate steel bar's surface and the magnesium potassium phosphate cement coating part. The formation process of iron (III) phosphate is believed to initiate from the bar coated with magnesium potassium phosphate cement paste and remained steady state during the process of the EC test. In addition to the stable properties of MKPC coating part, the excellent anti-corrosion performance of the MKPC paste coating is also attributed to the formation of a new passive layer that was iron (III) phosphate. This works holds promise that the MKPC coating may be affective in both repair and new construction applications.

## CRediT authorship contribution statement

**Fan Zhang:** Conceptualization, Methodology, Investigation, Formal analysis, Data curation, Writing – original draft, Visualization. **John J. Myers:** Conceptualization, Methodology, Investigation, Writing – original draft, Writing – review & editing, Visualization, Supervision, Project administration, Funding acquisition. **Wenyu Liao:** Investigation. **Cun Hui:** Investigation. **Hongyan Ma:** Conceptualization, Methodology, Investigation, Writing – review & editing, Funding acquisition.

## Declaration of Competing Interest

The authors declare that they have no known competing financial interests or personal relationships that could have appeared to influence the work reported in this paper.

## Data availability

Data will be made available on request.

## References

[1] C.B. Shin, E.K. Kim, Modeling of chloride ion ingress in coastal concrete, Cem. Concr. Res. 32 (5) (2002) 757–762.
[2] Koch, G.H., et al., *Corrosion cost and preventive strategies in the United States*. 2002, United States. Federal Highway Administration.
[3] De Sitter, W. *Costs of service life optimization" The Law of Fives"*. in *CEB-RILEM Workshop on Durability of Concrete Structures (Copenhagen, Denmark, May 18-20, 1983)*. 1984. Comité Euro-International du Béton.
[4] X. Shi, et al., Strength and corrosion properties of Portland cement mortar and concrete with mineral admixtures, Constr. Build. Mater. 25 (8) (2011) 3245–3256.
[5] J. Hou, D. Chung, Effect of admixtures in concrete on the corrosion resistance of steel reinforced concrete, Corros. Sci. 42 (9) (2000) 1489–1507.
[6] E. Sistonen, A. Cwirzen, J. Puttonen, Corrosion mechanism of hot-dip galvanised reinforcement bar in cracked concrete, Corros. Sci. 50 (12) (2008) 3416–3428.
[7] G. Parthiban, et al., Cathodic protection of steel in concrete using magnesium alloy anode, Corros. Sci. 50 (12) (2008) 3329–3335.
[8] F. Tang, G. Chen, R.K. Brow, Chloride-induced corrosion mechanism and rate of enamel-and epoxy-coated deformed steel bars embedded in mortar, Cem. Concr. Res. 82 (2016) 58–73.
[9] X. Feng, et al., The degradation of passive film on carbon steel in concrete pore solution under compressive and tensile stresses, Electrochim. Acta 58 (2011) 258–263.

[10] M. Behzadnasab, S. Mirabedini, M. Esfandeh, Corrosion protection of steel by epoxy nanocomposite coatings containing various combinations of clay and nanoparticulate zirconia, Corros. Sci. 75 (2013) 134–141.
[11] F. Tang, et al., Corrosion resistance and mechanism of steel rebar coated with three types of enamel, Corros. Sci. 59 (2012) 157–168.
[12] N. Etteyeb, et al., Corrosion protection of steel reinforcement by a pretreatment in phosphate solutions: assessment of passivity by electrochemical techniques, Corros. Eng. Sci. Technol. 41 (4) (2006) 336–341.
[13] D.G. Manning, Corrosion performance of epoxy-coated reinforcing steel: North American experience, Constr. Build. Mater. 10 (5) (1996) 349–365.
[14] Z.Q. Tan, C.M. Hansson, Effect of surface condition on the initial corrosion of galvanized reinforcing steel embedded in concrete, Corros. Sci. 50 (9) (2008) 2512–2522.
[15] M. Sánchez, et al., Electrochemical and analytical assessment of galvanized steel reinforcement pre-treated with Ce and La salts under alkaline media, Cem. Concr. Compos. 28 (3) (2006) 256–266.
[16] H. Ma, B. Xu, Z. Li, Magnesium potassium phosphate cement paste: Degree of reaction, porosity and pore structure, Cem. Concr. Res. 65 (2014) 96–104.
[17] N. Yang, et al., Research progresses in magnesium phosphate cement–based materials, J. Mater. Civ. Eng. 26 (10) (2014) 04014071.
[18] T. Zhang, L.J. Vandeperre, C.R. Cheeseman, Magnesium-silicate-hydrate cements for encapsulating problematic aluminium containing wastes, Journal of Sustainable Cement-Based Materials 1 (1–2) (2012) 34–45.
[19] F. Qiao, C. Chau, Z. Li, Property evaluation of magnesium phosphate cement mortar as patch repair material, Constr. Build. Mater. 24 (5) (2010) 695–700.
[20] J. Zhang, et al., Steel corrosion in magnesia–phosphate cement concrete beams, Mag. Concr. Res. 69 (1) (2017) 35–45.
[21] B. Abdelrazig, J. Sharp, B. El-Jazairi, The chemical composition of mortars made from magnesia-phosphate cement, Cem. Concr. Res. 18 (3) (1988) 415–425.
[22] H. Tang, et al., The protective effect of magnesium phosphate cement on steel corrosion, Constr. Build. Mater. 255 (2020), 119422.
[23] L. Jun, et al., Resistance to sulfate attack of magnesium phosphate cement-coated concrete, Constr. Build. Mater. 195 (2019) 156–164.
[24] B. Wang, et al., Study on anti-corrosion performance of silica fume modified magnesium potassium phosphate cement-based coating on steel, Case Stud. Constr. Mater. 17 (2022) e01467.
[25] L. Zhang, et al., Corrosion resistance of wollastonite modified magnesium phosphate cement paste exposed to freeze-thaw cycles and acid-base corrosion, Case Stud. Constr. Mater. 13 (2020) e00421.
[26] D. Wang, et al., Effect of magnesia-to-phosphate ratio on the passivation of mild steel in magnesium potassium phosphate cement, Corros. Sci. 174 (2020), 108848.
[27] Z. Ai, et al., Passive behaviour of alloy corrosion-resistant steel Cr10Mo1 in simulating concrete pore solutions with different pH, Appl. Surf. Sci. 389 (2016) 1126–1136.
[28] S. Ahmad, Reinforcement corrosion in concrete structures, its monitoring and service life prediction—a review, Cem. Concr. Compos. 25 (4–5) (2003) 459–471.
[29] V. Talakokula, et al., Diagnosis of carbonation induced corrosion initiation and progression in reinforced concrete structures using piezo-impedance transducers, Sens. Actuators, A 242 (2016) 79–91.
[30] C. Astm, ASTM G106–89, Standard Practice for Verification of Algorithm and Equipment for Electrochemical Impedance Measurements, American Society for Testing and Materials, USA, 2015.
[31] F. Tang, G. Chen, R.K. Brow, Chloride-induced corrosion mechanism and rate of enamel- and epoxy-coated deformed steel bars embedded in mortar, Cem. Concr. Res. 82 (2016) 58–73.
[32] Standard, A., *G61-86*. Standard test method for conducting cyclic potentiodynamic polarization measurements for localized corrosion susceptibility of iron-, nickel-, or cobalt-based alloys, ASTM standards, ASTM, Philadelphia, PA, USA, 2009.
[33] F. Tang, et al., Impact and corrosion resistances of duplex epoxy/enamel coated plates, Constr. Build. Mater. 112 (2016) 7–18.
[34] C. Astm, 876–09. Standard test method for corrosion potentials of uncoated reinforcing steel in concrete, American Society for Testing and Materials, USA, 2009.
[35] F. Tang, et al., Microstructure and corrosion resistance of enamel coatings applied to smooth reinforcing steel, Constr. Build. Mater. 35 (2012) 376–384.
[36] Wagh, A.S., *Chemically bonded phosphate ceramics: twenty-first century materials with diverse applications*. 2016: Elsevier.
[37] L. Jiang, et al., Influence of chloride salt type on threshold level of reinforcement corrosion in simulated concrete pore solutions, Constr. Build. Mater. 30 (2012) 516–521.
[38] C. Zhou, et al., Polybenzoxazine/SiO2 nanocomposite coatings for corrosion protection of mild steel, Corros. Sci. 80 (2014) 269–275.
[39] M. Behzadnasab, et al., Corrosion performance of epoxy coatings containing silane treated ZrO2 nanoparticles on mild steel in 3.5% NaCl solution, Corros. Sci. 53 (1) (2011) 89–98.
[40] H. Jamil, et al., Corrosion behaviour of reinforcing steel exposed to an amino alcohol based corrosion inhibitor, Cem. Concr. Compos. 27 (6) (2005) 671–678.
[41] A.L. Rudd, C.B. Breslin, F. Mansfeld, The corrosion protection afforded by rare earth conversion coatings applied to magnesium, Corros. Sci. 42 (2) (2000) 275–288.
[42] S.B. Aziz, et al., A conceptual review on polymer electrolytes and ion transport models, J. Sci.: Adv. Mater. Devices 3 (1) (2018) 1–17.
[43] P. Córdoba-Torres, T. Mesquita, R. Nogueira, Influence of geometry-induced current and potential distributions on the characterization of constant-phase element behavior, Electrochim. Acta 87 (2013) 676–685.
[44] P. Córdoba-Torres, et al., On the intrinsic coupling between constant-phase element parameters α and Q in electrochemical impedance spectroscopy, Electrochim. Acta 72 (2012) 172–178.
[45] M. Mahdavian, R. Naderi, Corrosion inhibition of mild steel in sodium chloride solution by some zinc complexes, Corros. Sci. 53 (4) (2011) 1194–1200.
[46] B. Hirschorn, et al., Determination of effective capacitance and film thickness from constant-phase-element parameters, Electrochim. Acta 55 (21) (2010) 6218–6227.
[47] A. Castela, et al., Influence of unsupported concrete media in corrosion assessment for steel reinforcing concrete by electrochemical impedance spectroscopy, Electrochim. Acta 124 (2014) 52–60.
[48] F. Tang, et al., Cement-modified enamel coating for enhanced corrosion resistance of steel reinforcing bars, Cem. Concr. Compos. 35 (1) (2013) 171–180.
[49] K. Sagoe-Crentsil, F. Glasser, J. Irvine, Electrochemical characteristics of reinforced concrete corrosion as determined by impedance spectroscopy, Br. Corros. J. 27 (2) (1992) 113–118.
[50] L. Chong, J. Yang, C. Shi, Effect of curing regime on water resistance of magnesium–potassium phosphate cement, Constr. Build. Mater. 151 (2017) 43–51.
[51] C. Monticelli, et al., Corrosion behaviour of a Low Ni austenitic stainless steel in carbonated chloride-polluted alkali-activated fly ash mortar, Cem. Concr. Res. 55 (2014) 49–58.
[52] M. Montemor, A. Simoes, M. Ferreira, Chloride-induced corrosion on reinforcing steel: from the fundamentals to the monitoring techniques, Cem. Concr. Compos. 25 (4–5) (2003) 491–502.
[53] *EC-lab Software Analysis and Data Process*. March 2020: p. 74.
[54] D. Cusson, et al., Corrosion-inhibiting systems for durable concrete bridges. I: Five-year field performance evaluation, J. Mater. Civ. Eng. 20 (1) (2008) 20–28.
[55] B. Xu, et al., Influence of magnesium-to-phosphate ratio and water-to-cement ratio on hydration and properties of magnesium potassium phosphate cements, Cem. Concr. Res. 123 (2019).
[56] V.S. Saji, H.-K. Song, LiFePO4 nanostructures fabricated from iron (III) phosphate (FePO4· 2H2O) by hydrothermal method, J. Nanosci. Nanotechnol. 15 (1) (2015) 734–741.
[57] A.P. Grosvenor, et al., Investigation of multiplet splitting of Fe 2p XPS spectra and bonding in iron compounds, Surf. Interface Anal. 36 (12) (2004) 1564–1574.
[58] M. Engelhard, et al., A Study of Potassium Dihydrogen Phosphate (KDP) Crystal Surfaces by XPS, Surf. Sci. Spectra 8 (1) (2001) 56–80.
[59] Y.-S. Lee, H.-T. Kim, K.-O. Yoo, Effect of ferric oxide on the high-temperature removal of hydrogen sulfide over ZnO-Fe2O3 mixed metal oxide sorbent, Ind. Eng. Chem. Res. 34 (4) (1995) 1181–1188.
[60] B.J. Tan, K.J. Klabunde, P.M. Sherwood, X-ray photoelectron spectroscopy studies of solvated metal atom dispersed catalysts. Monometallic iron and bimetallic iron-cobalt particles on alumina, Chem. Mater. 2 (2) (1990) 186–191.
[61] P. Mills, J. Sullivan, A study of the core level electrons in iron and its three oxides by means of X-ray photoelectron spectroscopy, J. Phys. D Appl. Phys. 16 (5) (1983) 723.
[62] J.A. Taylor, et al., Interactions of ion beams with surfaces. Reactions of nitrogen with silicon and its oxides, J. Chem. Phys. 68 (4) (1978) 1776–1784.
[63] G. Ertl, K. Wandelt, Electron spectroscopic studies of clean and oxidized iron, Surf. Sci. 50 (2) (1975) 479–492.
[64] G.C. Allen, et al., X-ray photoelectron spectroscopy of iron–oxygen systems, J. Chem. Soc. Dalton Trans. 14 (1974) 1525–1530.
[65] G.C. Allen, et al., X-ray photoelectron spectroscopy of some uranium oxide phases, J. Chem. Soc. Dalton Trans. 12 (1974) 1296–1301.
[66] V. Shah, et al., Changes in microstructure characteristics of cement paste on carbonation, Cem. Concr. Res. 109 (2018) 184–197.
[67] A.B. Revert, et al., Carbonation-induced corrosion: Investigation of the corrosion onset, Constr. Build. Mater. 162 (2018) 847–856.
[68] J. Taylor, et al., X-ray powder diffraction analysis of cements, Structure and performance of cements (2002) 420–441.
[69] Grier, D. and G. McCarthy, *North Dakota state university*. Fargo, North Dakota, USA, ICDD grant-in-aid, 1991.
[70] J. Hanawalt, H. Rinn, L. Frevel, Chemical analysis by X-ray diffraction, Ind. Eng. Chem. Anal. Ed. 10 (9) (1938) 457–512.
[71] H. Bassett, W.L. Bedwell, 212. Studies of phosphates. Part III. Some complex orthophosphates of sodium and a bivalent metal, and some orthophosphate solid solutions, Journal of the Chemical Society (Resumed) (1933) 877–882.
[72] S. Endo, et al., Pressure-induced transition of the hydrogen bond in the ferroelectric compounds KH 2 P0 4 and KD 2 P0 4, Nature 340 (6233) (1989) 452–455.
[73] J. Borensztajn, Structures cristallines de la métavariscite et de la métastrengite, Bull. Minér. 89 (4) (1966) 428–438.
[74] H. Chessin, W.C. Hamilton, B. Post, Position and thermal parameters of oxygen atoms in calcite, Acta Crystallogr. 18 (4) (1965) 689–693.
[75] J. Jeffery, The crystal structure of tricalcium silicate, Acta Crystallogr. 5 (1) (1952) 26–35.
[76] O. Chaix-Pluchery, et al., Structural prereactional transformations in Ca (OH) 2, J. Solid State Chem. 67 (2) (1987) 225–234.
[77] H. Midgley, A compilation of X-ray powder diffraction data of cement minerals, Mag. Concr. Res. 9 (25) (1957) 17–24.
[78] C.S. Hurlbut Jr, J.L. Baum, Ettringite from Franklin, New Jersey, American Mineralogist: Journal of Earth and Planetary Materials 45 (11–12) (1960) 1137–1143.